Study of QED radiative corrections to charged lepton leg in neutrino-nucleon interactions

Pueh Leng Tan

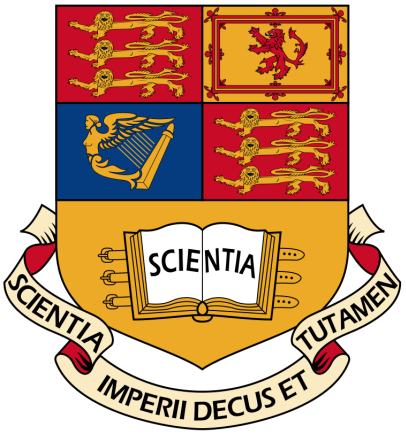

Department of Theoretical Physics
Imperial College London

Submitted in partial fulfillment of the requirements for the degree of Masters of Science in Theoretical Physics from Imperial College London

Supervised by Dr. Morgan Wascko

Last compiled on September 20, 2013

Abstract

There is a recent renewal of interest to include radiative corrections to neutrino charged-current quasi-elastic(CCQE) scattering into modern neutrino interaction generators[1][2]. This piece of work serves as a preliminary study of the significance of such radiative corrections for the T2K experiment. The theoretical background relevant to the discussion of such QED radiative corrections is provided by a brief review on Fermi's four-fermion theory, Glashow-Salam-Weinberg theory, neutrino oscillations and the see-saw mechanism. Using the T2K experiment's muon neutrino flux predictions at the Super-Kamiokande detector, radiative corrections to muon neutrino CCQE events were calculated. Calculation of the radiative corrections required information about the double differential cross-section of the interaction. This is extracted from Monte Carlo CCQE events generated using a neutrino interaction generator, NEUT. The radiative corrections at the peak muon energy at the SK detector is found to be -22.41% which is not small but further detailed investigations are required before comparing it to the observed discrepancy between data and simulations.

Acknowledgements

I would like to thank my supervisor, Dr Morgan Wascko for his guidance and support throughout this MSc project. I have been wanting to work on neutrinos since some time back, but due to some strange twist of karma, I ended up working on other types of particles. Thus, I am really grateful for this opportunity to work on neutrinos and learn more about them. They are truly cute and awesome particles.

I would also like to thank Dr Per Jonsson for his help with NEUT and his advice when I did not have a clear idea of where to take this project. I would like to thank Peter Sinclair for his expert advice on NEUT and tidbits about neutrino physics in general. I am also thankful towards Ben Krikler for his help and interesting conversations we had about coding. I am also grateful towards my fellow MSc students Alexander Hild and Mahesh Vidhyadharan for all the fruitful and fun discussions we had about neutrino cross-sections and other random things.

Lastly, I would like to thank my friend, Hui Han Chin, for technical and moral support.

Declaration

I declare that the work in this dissertation was carried out in accordance with the requirements of the University's Regulations and Code of Practice for Taught Postgraduate Programmes and that it has not been submitted for any other academic award. Except where indicated by specific reference in the text, this work (including figures) is my own work. Where I have quoted from the work of others, I have included the source in the references. Any views expressed in the dissertation are those of the author.

Pueh Leng Tan

List of Tables

4.1 Types of neutrino oscillation experiments with their typical sensitivity to Δm^2_{ij} 28

7.1 Important input parameters for NEUT. The input card codes found in Appendix B shows the full list of input parameters and options available in NEUT. The full analysis code and shell scripts are available upon request. . 51

C.1 Percentage of problematic events for the Various binning schemes. The binning scheme (6 MeV/bin, 2e-2/bin) gives the smallest percentage of problematic events while not compromising on the accuracy of the calculation. . 68

C.2 Percentage of problematic events for the various Z binning schemes. Varying the Z bin size does not affect the percentage of problematic events drastically. 68

C.3 Fractional radiative corrections for ν_μ CCQE interactions. Table shows value of each bin in figure 7.4, expressed as a percentage. 69

List of Figures

3.1 Triangle anomaly 18

4.1 Neutrinoless double β-decay 31

5.1 Schematic of the T2K experiment. The neutrinos travelled 295 km through the Earth from the J-PARC source to the Super-Kamiokande detector. Figure taken from [3] 32
5.2 Tree-level charged-current quasi-elastic(CCQE) neutrino scattering 34
5.3 Example of a muon-like event detected at the SK detector. Image taken from [4] 35
5.4 The proton and neutron potential wells and energy levels within the nucleus. The binding energy and Fermi momentum are adjusted with experimental data. Figure taken from [5] 40

6.1 $\mathcal{O}(\alpha)$ corrections to tree-level cross-section come from interference of these diagrams with tree-level diagram. 41
6.2 Low energy neutrinos interact with the bound nucleons and all the details of the interaction are represented by the grey blob, $\mathcal{M}_0$, which is a function of the momentum transfer. 42
6.3 QED vertex up to one-loop corrections 44
6.4 First order vertex correction 44
6.5 a: lepton leg bremsstrahlung, b: lepton propagator self-energy, c: interference, d: hadron leg bremsstrahlung, e: hadron propagator self-energy, f,g: two-boson exchange, h: gauge boson self-interactions. 47

7.1 Muon neutrino flux prediction at the SK detector. Data taken from [4]. The flux can be split into three regions. Most of the muon neutrinos have energies below 2 GeV, a substantial amount of them have energies from 2 GeV to 10 GeV and a trace amount have energies above 10 GeV but below 23 GeV. The flux is peaked at 0.6 GeV. 52
7.2 θ is the deflection angle between the incoming neutrino and outgoing muon, while E_μ is the outging muon energy. The z-axis gives the cross-section(cm^2) for muon neutrino CCQE scattering in each bin in the event kinematics space. 53
7.3 Problematic events at high Q^2. The boxes reflect the distribution of type II problematic events. The line overlaid is a curve constant neutrino energy, $E_\nu = 0.6$ GeV, and constant momentum transfer, $\sqrt{Q^2} = 0.8$ GeV. Most of the CCQE events have momentum transfer $\sim \sqrt{Q^2} = 0.4$ GeV. 54

7.4 The fractional radiative corrections as defined in equation 7.3 is represented by the z-axis. The value of the radiative corrections in each bin can be found in table C.3 in Appendix C. 56

Contents

1 Introduction **6**

2 Fermi theory **8**
2.1 Fermi current-current Lagrangian 8
2.2 V-A structure 9
2.3 Leptonic currents 10
2.4 Hadronic current 10
2.4.1 CVC hypothesis 10
2.4.2 PCAC hypothesis 11
2.5 Status of Fermi theory 12

3 Glashow-Salam-Weinberg theory **14**
3.1 GSW Lagrangian 14
3.2 Gauge fields 14
3.3 Fermionic matter fields 15
3.4 Scalar fields 15
3.4.1 Spontaneous Symmetry Breaking 16
3.4.2 Higgs Mechanism 17
3.5 Yukawa coupling 17
3.6 Anomalies and Renormalisability 18
3.7 Status of GSW theory 19

4 Neutrino Physics **21**
4.1 Massive neutrinos 21
4.1.1 Dirac mass 22
4.1.2 Majorana mass 22
4.1.3 See-saw mechanism 23
4.2 Neutrino Oscillations 24
4.2.1 Plane-wave derivation 24
4.2.2 Comments on neutrino oscillation probabilities 26
4.2.3 Antineutrino transition probability 27
4.2.4 Types of neutrino oscillation experiments 28
4.2.5 Appearance vs Disappearance experiments 29
4.2.6 Pontecorvo-Maki-Nakagawa-Sakata(PMNS) matrix 29
4.3 Open questions 30

5 T2K experiment **32**
5.1 Physics goals . . . 33
5.2 Neutrino detection . . . 34
5.3 Neutrino interactions . . . 35
5.3.1 Llewellyn-Smith formalism for neutrino-free nucleon scattering . . . 35
5.4 Nuclear environment . . . 39
5.4.1 Relativistic Fermi Gas (RFG) model . . . 39
5.4.2 Pauli blocking . . . 40

6 Radiative corrections in QED **41**
6.1 Bremsstrahlung . . . 42
6.2 Electron vertex modification . . . 43
6.3 Radiative corrections to neutrino scattering . . . 46
6.4 Contributing diagrams . . . 47
6.5 Leading log approximation . . . 48
6.6 Double differential cross-section . . . 49

7 Simulations **50**
7.1 Software . . . 50
7.1.1 NEUT . . . 50
7.2 Code structure and Findings . . . 51
7.2.1 Double differential cross-section . . . 51
7.2.2 Optimisation . . . 53
7.2.3 Radiative correction calculations . . . 55
7.3 Conclusions . . . 57
7.4 Recommendations . . . 57

A Useful mathematical tools **58**
A.1 Gamma matrix properties . . . 58
A.2 $SU(2) \times U(1)$ generators . . . 59
A.3 Feynman Parameters . . . 59
A.4 Regularisation schemes . . . 60
A.5 Wick rotation . . . 61

B NEUT card file **62**

C Data tables **68**
C.1 Optimising binning schemes . . . 68
C.2 Values of fractional radiative corrections . . . 69

Chapter 1

Introduction

This dissertation presents a study of the QED radiative corrections to neutrino charged-current quasi-elastic interactions, which is the dominant interaction via which neutrinos are detected in neutrino oscillation experiments. The first attempt to calculate the radiative corrections to neutrino scatterings dates back to the early 1970s by Kiskis[6]. This was shortly after the advent of the Glashow-Salam-Weinberg(GSW) theory which unified electromagnetism and the weak interactions. The calculations for non-elastic neutrino scatterings were cumbersome and heavily dependent on the parton models used to describe the nucleons that the neutrinos interact with. Nevertheless, this calculations was made more tractable by de Rujula in the late 1970s by taking leading approximations. Even though interests in this area of research continued into the early 1980s, radiative corrections are not incorporated into modern neutrino interaction event generators used in neutrino experiments.

There is a renewal of interest in recent years because neutrino experiments are approaching sensitivities at which radiative corrections are significant. A study in 2012 suggested that radiative corrections contribute a surprisingly large difference of $\sim 10\%$ to the difference between cross-sections of the electron neutrino and muon neutrino at the energies from 200 MeV to 2 GeV, which is of interest to neutrino oscillation experiments. This is comparable to the current systematic uncertainties at accelerator neutrino experiments such as the T2K experiment[1]. This finding remains to be confirmed by a full calculation implemented inside a generator, thus motivating this study.

It is important to consider radiative effects in neutrino oscillations analysis as emission of soft photons by the outgoing charged leptons can alter the topology of the event and lead to uncertainties in the reconstruction of the kinematical variables[2]. Hard photons emitted by muons can be mistaken for electron neutrino events[7]. This is undesirable as it is a source of unaccounted background events for experiments that search for $\nu_\mu \to \nu_e$ oscillations, such as the T2K experiment. In this study, the radiative corrections to muon neutrino CCQE interactions are simulated according to the setup of the T2K experiment. This serves as a preliminary study of the significance of radiative corrections in current experiments so that efforts can be channelled into including them into modern

generators.

This dissertation is structured as follow:

Chapter 2 provides a concise overview of weak interaction phenomenology by starting with the Fermi four-fermion theory and introducing the V-A structure of the weak leptonic and hadronic currents. A common approach in effective field theories is to use form factors to package the properties of particle interactions without including all of the underlying physics. There are some brief words on why Fermi theory is not the ultimate description of nature and why it is still in use today anyway.

Chapter 3 introduces the GSW theory and the basic features of its Lagrangian, such as its matter content, and roles of the gauge bosons and scalar fields. Spontaneous symmetry breaking in the Electroweak sector and how fermions and boson acquire their masses is explained, along with a few comments about the renormalisibility of the GSW theory.

Chapter 4 is about neutrino physics and how the Standard Model can be minimally extended to give neutrinos masses. The different types of neutrino masses and the mechanism that can potentially give neutrinos masses will be elaborated on, along with the most direct implication of neutrino masses - ocillations. The chapter contains derivations of neutrino oscillations and explains how one may try to understand neutrino oscillations experimentally. The current status of the measurement of oscillation parameters is summarised, along with some words on the planned experiments to answer some of those open questions in neutrino physics.

Chapter 5 introduces the T2K experiment. The chapter also includes the derivation of the neutrino CCQE cross-section and discusses how the nuclear environment of the target nuclei is modelled.

Chapter 6 explains what radiative corrections are considered. The potential problems, such as infrared divergences, encountered when evaluating the radiative corrections are elaborated on, along with how these divergences are cancelled when considering physical processes. The chapter also introduces the concept of 'inclusive cross-section' and why they are more relevant in experiments than the bare tree-level cross-section. The expression for the radiative corrections is annotated, along with some comments on the assumptions made to render the calculation tractable.

Lastly, chapter 7 describes the details of the simulation, such as the softwares used and the structure of the code. The results are presented, along with the conclusions and recommendations for future work.

Chapter 2

Fermi theory

Fermi theory was introduced in 1934 to describe weak interaction and to explain beta decay in particular[8]. It only contains one type of vertex in which four fermions interact with each other at the same point. This implies an infinitesimal interaction length, which is a good approximation of a theory with very massive intermediate vector boson. This is indeed the case, but the existence of the massive vector boson was not proposed at the time the theory was first constructed.

As a phenomenological theory, Fermi's four-fermion theory describes the weak interaction very well but it has serveral short-comings which eventually proved that it is not the ultimate description of nature. Nevertheless, it is still widely used by experimentalists as the theory remains a very good approximation at the energies at which modern experiments are being carried out[9].

2.1 Fermi current-current Lagrangian

Fermi theory is called the current-current theory as the Lagrangian involves two local currents, J^α, which exist at the same point in spacetime. This defines a four-fermion interaction and there are no intermediate vector bosons, yet.

$$\mathcal{L}_F = -\frac{G_F}{\sqrt{2}} J^\alpha(x) J^\dagger_\alpha(x) \tag{2.1}$$

where

$$J^\alpha(x) = l^\alpha(x) + h^\alpha(x) \tag{2.2}$$

$$G_F = 1.166 \times 10^{-5}\ \text{GeV}^{-2} \tag{2.3}$$

There is only one coupling constant, G_F, which is known as Fermi's constant. It has dimensions of energy^{-2} which renders the theory unrenormalisable by the power counting theorem[10]. This means that some physical quantities, such as the cross-section of a process, can potentially diverge and make the theory unphysical.

The weak current consists of a leptonic part, l^α, and a hadronic part, h^α. As such, the Fermi Legrangian produces three kinds of interactions. The first kind of interaction is leptonic in nature and corresponds to terms like $l^\alpha l^\dagger_\alpha$. This is responsible for processes such as the decay of the muon.

$$\mu^- \to e^- + \bar{\nu}_e + \nu_\mu$$

There is also the hadronic interaction which corresponds to the $h^\alpha h^\dagger_\alpha$ term and is responsible for processes such as the decay of the Lambda baryon.

$$\Lambda \to p + \pi^-$$

Lastly, there is the semileptonic interactions which correspond to terms like $l^\alpha h^\dagger_\alpha + h^\alpha l^\dagger_\alpha$ and cause processes like neutron decay.

$$n \to p + e^- + \bar{\nu}_e$$

2.2 V-A structure

The weak force couples only to left-handed neutrinos (and right-handed antineutrinos). To accommodate for parity and charge conjugation violation, the current must have the vector minus axial (V-A) structure. This was introduced independently by Feynman and Gell-mann, and Sudarshan and Marshak in 1958[11][12]. A generic four-fermion interaction $A + B \to C + D$ is described by a universal four-fermion matrix element

$$\mathcal{M} = 4 \sum_i f_i \left\langle \overline{\Psi^L_D} \right| \mathcal{O}_i \left| \Psi^L_B \right\rangle \left\langle \overline{\Psi^L_C} \right| \mathcal{O}_i \left| \Psi^L_A \right\rangle \tag{2.4}$$

where

$$\Psi^L = a\Psi = \frac{1}{2}(1 - \gamma_5)\Psi \tag{2.5}$$

The sum is over the same operator $\mathcal{O}_i$ and the f_i are coupling constants. A and B represent the 'in' states, while C and D represent the 'out' states.

Considering all possible types of bilinear operators, $\bar{a}\mathcal{O}_i a$,

Scalar	$\bar{a}a = 0$	
Vector	$\bar{a}\gamma_\mu a = \gamma_\mu a$	
Axial-vector	$\bar{a}\gamma_\mu\gamma_5 a = -\gamma_\mu a$	(2.6)
Pseudoscalar	$\bar{a}\gamma_5 a = 0$	
Tensor	$\bar{a}\sigma_{\mu\nu}\gamma_5 a = 0$	

Substituting equation 2.6 into equation 2.4,

$$\mathcal{M}(A + B \to C + D) = \frac{G_F}{\sqrt{2}} \left\langle \overline{\Psi_D} \right| \gamma^\mu(1 - \gamma_5) \left| \Psi_B \right\rangle \left\langle \overline{\Psi_C} \right| \gamma_\mu(1 - \gamma_5) \left| \Psi_A \right\rangle \tag{2.7}$$

Only the vector and axial-vector bilinears survive because the weak force only couples to left-handed fermions (right-handed anti-fermions).

2.3 Leptonic currents

Charged lepton flavour is conserved as there are no cross-terms between charged leptons and neutrinos from different generations.

$$l^{\alpha}(x) = \sum_{\text{generations}} \bar{l}(x)\gamma^{\alpha}(1-\gamma_5)\nu_l(x) \tag{2.8}$$

where the leptonic current sums over all three generations of leptons. An example of the matrix element describing the leptonic current in neutrino-electron scattering is

$$\langle e|\, l^{\alpha}\, |\nu_e\rangle \simeq \bar{u}_e\gamma^{\alpha}(1-\gamma_5)u_{\nu} \tag{2.9}$$

where $\bar{u}_e$ and u_{ν} are Dirac spinors which are approximately chiral eigenvectors if the initial neutrino is ultra-relativistic. This transition has a change in charge, $\Delta Q = -1$, which is why processes involving such lepton legs are called charged-current interactions.

2.4 Hadronic current

The hadronic leg is more complicated than the leptonic leg. Unlike the charged leptons and neutrinos, hadrons are affected by strong interactions and do not behave like point particles. However, the mathematical structure of the hadronic current is similar to that of the leptonic current. For example, the matrix element used to describe the hadronic leg in β decay is given by

$$\langle p|\, h^{\alpha}\, |n\rangle \simeq \bar{u}_p\gamma^{\alpha}(g_V - g_A\gamma_5)u_n \tag{2.10}$$

where g_V and g_A are known as the vector coefficient and axial-vector coefficient respectively. They are experimentally measured to be $g_V \simeq 0.98$ and $g_A \simeq 1.27$. The hadronic current will have exactly the same structure as the leptonic current if the ratio $\frac{g_V}{g_A}$ were to be exactly unity. A priori, there is no reason to expect the hadronic current to be so similar to the leptonic current since the strong interactions can modify the vector and axial-vector part of the current separately. This similarity is explained by the conserved vector current (CVC) and partially conserved axial current (PCAC) hypothesis.

2.4.1 CVC hypothesis

The CVC hypothesis is first proposed by Gerstein and Zeldovich in 1956 and it assumes that the vector current is a component of a conserved isovector current[13]. The conservation of this current prevents the hadronic weak vertex from being renormalised by the strong interactions. The CVC hypothesis was experimentally verified in 1963 by

measurements of the shape correction factor of the B^{12} and N^{12} nucleus β spectrum[14]. Examining the vector part of the hadronic leg in a β-decay,

$$V^{\alpha} = \langle p| \gamma^{\alpha} |n\rangle \tag{2.11}$$

The general form of V^{α} is restricted by Lorentz symmetry to be

$$V^{\alpha} = \bar{u}_p \left[g_V \gamma^{\alpha} - i \frac{g_M}{2M} \sigma^{\alpha\beta} q_{\beta} - \frac{g_S}{2M} q^{\alpha} \right] u_n \tag{2.12}$$

where the form factors g_V, g_M, g_S are functions of the momentum transfer, q^2. The CVC hypothesis leads to the condition

$$q^{\alpha} V_{\alpha} = 0 \tag{2.13}$$

which then implies that $g_S = 0$ and equation 2.12 simplifies to

$$V^{\alpha} = \bar{u}_p \left[g_V \gamma^{\alpha} - i \frac{g_M}{2M} \sigma^{\alpha\beta} q_{\beta} \right] u_n \tag{2.14}$$

The first term in equation 2.14 is the vector term which dominates if the nucleons are not strongly interacting particles. The second term is the weak magnetism term which determines the deviations from the allowed shape of the observed β spectra for the B^{12} and N^{12} decays. Measurements of this shape deviation strongly supports the CVC hypothesis.

2.4.2 PCAC hypothesis

The axial vector coefficient only deviates $\sim 25\%$ from unity because of the PCAC hypothesis. The deviation is bigger for the axial-vector coefficient than for the vector coefficient as the axial-vector current is only partially conserved. In 1964, Adler proposed a way to test the PCAC hypothesis by comparing cross-sections of the following interactions

high-energy neutrino interactions	$\nu + \alpha \rightarrow l + \beta$
pion-hadron interactions	$\pi^{+} + \alpha \rightarrow \beta$

where α is a nucleon or nucleus, l is the corresponding charged lepton of the ν, β is a system of strongly interacting particles with a different invariant mass from α. The incoming neutrino is ultra-relativistic and lepton mass is neglected[15].

When the momentum transfer is small, the resulting charged lepton is mainly forward moving and the matrix element for the high-energy neutrino interaction is proportional to the divergence of the axial vector current, provided that the CVC hypothesis holds. Under the PCAC hypothesis, the cross-section of the high-energy neutrino interaction is proportional to the cross-section of pion-hadron interactions. This was empirically verified in 1969 by Bonetti et al. as their data was consistent with the PCAC hypothesis in the low momentum transfer regime[16].

In fact, the proportionality constant relating the cross-sections of the two interactions vanishes in the limit of vanishing pion mass.

$$\begin{aligned} \partial_\alpha A_i^\alpha(x) &= f_\pi m_\pi^2 \pi_i(x) \\ \lim_{m_\pi \to 0} \partial_\alpha A^\alpha &= 0 \end{aligned} \tag{2.15}$$

where $A_i^\alpha(x)$ is the axial current, f_π is the pion decay constant, m_π is the charged pion mass and $\pi_i(x)$ is the pseudoscalar field operator. Modern experiments give a measurement of $m_\pi \sim 140$ MeV and this further supports the hypothesis that the axial current is not fully conserved[17].

2.5 Status of Fermi theory

Since its formulation in 1934, there were several modifications to the Fermi's four-fermion theory so that it can describe the weak force more accurately. Fermi theory, along with those modifications, served well as a phenomenological theory. It withstood the verifications of numerous experiments since its formulation in the 1934 before it was superceded by the Glashow-Salam-Weinberg theory in the 1960s.

The greatest set-back of Fermi theory is that it violates unitarity at high energies and it is not renormalisable. For example, consider the reaction $\nu_e + e \to e + \nu_e$. Assuming ultra-relativistic electrons, the calculated cross-section in the center-of-mass system grows as [18]

$$\sigma = \frac{4G_F^2 k^2}{\pi} \simeq G_F^2 E_{CM}^2. \tag{2.16}$$

The cross-section is unbounded as it grows with the center-of-mass energy. The theory violates unitarity and it breaks down at $E_{CM} \simeq G_F^{-1/2} \simeq 300$GeV. However, this energy is considered high given that current experiments, such as the T2K experiment, have E_{CM} on the order of ~ 1 GeV, and hence the Fermi theory remains a good approximation for the analysis of modern experiments.

One can hope to handle the diverging cross-section by absorbing it into the definitions of the coupling constants, charge and normalisation of the fields. However, Fermi theory is not renormalisable as G_F has a dimension of energy^{-2} and is not renormalisable by power counting. To solve this problem, Schwinger introduced intermediate vector bosons to the theory in 1957 [19]. The four-fermion vertex was split up by introducing intermediate vector bosons via the Lagrangian

$$\mathcal{L} = g_W [J^\alpha(x) W_\alpha^+(x) + J^{\alpha\dagger}(x) W_\alpha^-(x)] \tag{2.17}$$

$$\frac{g_W^2}{m_W^2} = \frac{G_F}{\sqrt{2}} \tag{2.18}$$

where $W_\alpha^\pm(x)$ are the intermediate vector bosonic fields and m_W is the mass of the $W^\pm$ boson.

Equation 2.18 suggests that the new coupling strength, g_W, is dimensionless and the theory with intermediate vector bosons is thus superficially renormalisable. However, it is still problematic for scattering processes such as $\bar{\nu}\nu \rightarrow W^+W^-$ and $e^+e^- \rightarrow W^+W^-$. The W propagator approaches a constant at high energies and the cross-sections of these proccesses diverge as E^2_{CM}[20].

The intermediate vector bosons Schwinger proposed are massive given the short interaction length and point-like nature of the vertex. However, the vector bosons in Fermi theory are massless since explicit mass terms will break gauge invariance. The vector bosons eventually acquired masses via the Higgs mechanism in the framework of the Glashow-Salam-Weinberg electroweak theory that is widely used today.

Chapter 3

Glashow-Salam-Weinberg theory

3.1 GSW Lagrangian

The Glashow-Salam-Weinberg (GSW) theory describes the unification of electromagnetism and the weak interaction. It is a gauge theory based on the product group $SU(2)_W \times U(1)_Y$ which is subsequently spontaneously broken down to $U(1)_{EM}$. The Lagrangian density is

$$\mathcal{L} = \mathcal{L}_g + \mathcal{L}_f + \mathcal{L}_s + \mathcal{L}_{f-s} \tag{3.1}$$

where $\mathcal{L}_g$ describes the gauge fields in the theory, $\mathcal{L}_f$ describes the fermionic matter content, $\mathcal{L}_s$ comes from the contribution of the scalar fields and $\mathcal{L}_{f-s}$ is the Yukawa coupling between the scalar and fermionic fields.

3.2 Gauge fields

Due to the product group structure of the theory, there are two field strength tensors, $f_{\mu\nu}$ and $F^j_{\mu\nu}$. The dimension of $SU(2)_W \times U(1)_Y$ is four and there are four gauge bosons: $\boldsymbol{b}_\mu \equiv (b^1_\mu, b^2_\mu, b^1_\mu)$ for $SU(2)_W$ and a_μ for $U(1)_Y$. They all transform under the adjoint representation of their respective groups. The gauge field Lagrangian subsequently gives the propagators of the gauge bosons.

$$\mathcal{L}_g = -\frac{1}{4} F^j_{\mu\nu} F^{\mu\nu}_j - \frac{1}{4} f_{\mu\nu} f^{\mu\nu} \tag{3.2}$$

The Abelian field strength tensor associated with weak hypercharge, $U(1)_Y$, is

$$f_{\mu\nu} = \partial_\mu a_\nu - \partial_\nu a_\mu \tag{3.3}$$

While the non-Abelian field strength tensor associated with the weak isospin, $SU(2)_W$, is

$$F^j_{\mu\nu} = \partial_\mu b^j_\nu - \partial_\nu b^j_\mu - g\epsilon_{jkl} b^k_\mu b^l_\nu \tag{3.4}$$

3.3 Fermionic matter fields

The Lagrangian associated with the fermions is only explicitly written out for the electron and electron neutrino. The other generations of leptons have the same structure as well.

$$\mathcal{L}_f = \bar{R} i\gamma^\mu(\partial_\mu + \frac{ig'}{2}a_\mu y)R + \bar{L} i\gamma^\mu(\partial_\mu + \frac{ig'}{2}a_\mu y + \frac{ig}{2}\boldsymbol{\tau}\cdot\boldsymbol{b}_\mu)L \tag{3.5}$$

The left and right-handed leptons are defined via the projection operator $\frac{1}{2}(1 \pm \gamma_5)$.

$$\begin{aligned} R &\equiv e_R = \frac{1}{2}(1+\gamma_5)e \\ L &\equiv \begin{pmatrix}\nu \\ e\end{pmatrix}_L = \frac{1}{2}(1-\gamma_5)\begin{pmatrix}\nu \\ e\end{pmatrix} \end{aligned} \tag{3.6}$$

There are two independent couplings: the weak isopin coupling, g, and the weak hypercharge coupling, $\frac{g'}{2}$, and the weak isopin only couples to the left-handed leptons. Explicit mass terms are not allowed as they are incompatible with gauge invariance. The fermions eventually get their masses via the Higgs mechanism after spontaneous symmetry breaking.

3.4 Scalar fields

The scalar sector is where spontaneous symmetry breaking occurs and three of the gauge bosons acquire their masses via the Higgs mechanism.

$$\mathcal{L}_s = (D^\mu\phi)^\dagger(D_\mu\phi) - V(\phi^\dagger\phi) \tag{3.7}$$

where the transformation properties of the scalar field ϕ can be inferred from the definition of the covariant derivative

$$D_\mu = \partial_\mu + \frac{ig'}{2}a_\mu y + \frac{ig}{2}\boldsymbol{\tau}\cdot\boldsymbol{b}_\mu \tag{3.8}$$

The potential used to spontaneously break the symmetry is

$$V(\phi^\dagger\phi) = \mu^2\phi^\dagger\phi + \lambda(\phi^\dagger\phi)^2, \qquad \lambda > 0 \tag{3.9}$$

The charged leptons and three of the gauge bosons acquire their masses via the Higgs mechanism. The most economical and consistent choice of scalars is a complex SU(2) doublet.

$$\phi = \begin{pmatrix}\phi^+ \\ \phi^0\end{pmatrix} = \frac{1}{\sqrt{2}}\begin{pmatrix}\phi_1 + i\phi_2 \\ \phi_3 + i\phi_4\end{pmatrix} \tag{3.10}$$

3.4.1 Spontaneous Symmetry Breaking

The local gauge symmetry is broken by imposing a 'tachyonic' mass term for the scalars $\mu^2 < 0$ and picking a specific vacuum expectation value for the scalar field.

$$\langle\phi\rangle_0 \equiv \langle 0|\,\phi\,|0\rangle = \begin{pmatrix} 0 \\ \frac{v}{\sqrt{2}} \end{pmatrix} \tag{3.11}$$

$$v = \sqrt{\frac{-\mu^2}{\lambda}} \tag{3.12}$$

The generators of the SU(2) algebra are $t_i \equiv \frac{\sigma_i}{2}$, where σ_i are the Pauli matrices while the U(1) generator, y, is just the identity matrix (see A.2). The four generators for $SU(2) \times U(1)$ mix and form a new set of generators (τ_1, τ_2, K, Q).

$$K \equiv \frac{\tau_3 - y}{2}, \qquad Q \equiv \frac{\tau_3 + y}{2} \tag{3.13}$$

Q is the electric charge and it relates the third component of the weak isopin with the weak hypercharge via

$$Q = t_3 + \frac{y}{2} \tag{3.14}$$

Recall the vacuum stability condition

$$(t_{\hat{\imath}})_{ab}\,\bar{\phi}_b = 0 \tag{3.15}$$

where $t_{\hat{\imath}}$ are the generators of the stability subgroup, and act the generators on the choice of vacuum given in 3.11,

$$\begin{aligned} \tau_1\,\langle\phi\rangle_0 &= \begin{pmatrix} \frac{v}{\sqrt{2}} \\ 0 \end{pmatrix} \neq 0 \\ \tau_2\,\langle\phi\rangle_0 &= \begin{pmatrix} \frac{-iv}{\sqrt{2}} \\ 0 \end{pmatrix} \neq 0 \\ K\,\langle\phi\rangle_0 &= \begin{pmatrix} 0 \\ \frac{-v}{\sqrt{2}} \end{pmatrix} \neq 0 \\ Q\,\langle\phi\rangle_0 &= \begin{pmatrix} 0 \\ 0 \end{pmatrix} \end{aligned} \tag{3.16}$$

For each generator that does not annihilate the vacuum, there is a would-be massless Goldstone boson. This is undesirable since massless scalars are not observed in reality. This disaster is averted by reparameterising ϕ and going into the unitary gauge. The Goldstone fields then are absorbed into the gauge fields and reincarnate as mass terms for those gauge bosons.

3.4.2 Higgs Mechanism

ϕ can be reparameterised as[21]

$$\phi(x) = e^{i\frac{\boldsymbol{\xi}\cdot\boldsymbol{\tau}}{2v}} \begin{pmatrix} 0 \\ \frac{v+\eta(x)}{\sqrt{2}} \end{pmatrix} \equiv U^{-1}(\boldsymbol{\xi}) \begin{pmatrix} 0 \\ \frac{v+\eta}{\sqrt{2}} \end{pmatrix} \tag{3.17}$$

Going into the unitary gauge and noting that the gauge fields, $\boldsymbol{b}_\mu$, transform in the adjoint representation,

$$\begin{aligned} &\phi \to \phi' = U(\boldsymbol{\xi})\phi = \frac{1}{\sqrt{2}} \begin{pmatrix} 0 \\ v+\eta \end{pmatrix} \\ &\boldsymbol{\tau}\cdot\boldsymbol{b}_\mu \to \boldsymbol{\tau}\cdot\boldsymbol{b}'_\mu \qquad\qquad a_\mu \to a_\mu \\ &R \to R \qquad\qquad L \to L' = U(\boldsymbol{\xi})L \end{aligned} \tag{3.18}$$

Substituting 3.18 into 3.7 and repackaging the terms,

$$\mathcal{L}_s = \frac{1}{2}(\partial^\mu\eta)(\partial_\mu\eta) - \frac{1}{2}m_\eta^2\eta^2 + \frac{1}{2}m_W^2\left(|W_\mu^+|^2 + |W_\mu^-|^2\right) + \frac{1}{2}m_Z^2|Z_\mu^0|^2 + \text{interaction terms} \tag{3.19}$$

where the physical gauge bosons are

$$W_\mu^+ \equiv \frac{1}{\sqrt{2}}(b_\mu^1 - ib_\mu^2) \qquad W_\mu^- \equiv \frac{1}{\sqrt{2}}(b_\mu^1 + ib_\mu^2) \tag{3.20}$$

$$Z_\mu^0 \equiv \frac{-g'a_\mu + gb_\mu^3}{\sqrt{g^2+g'^2}} \qquad A_\mu \equiv \frac{ga_\mu + g'b_\mu^3}{\sqrt{g^2+g'^2}} \tag{3.21}$$

with masses

$$m_\eta \equiv \sqrt{-2\mu^2} \qquad m_W = \frac{gv}{2} \qquad m_Z = m_W\sqrt{1+\left(\frac{g'}{g}\right)^2} \tag{3.22}$$

Looking at equations 3.16, three of the $SU(2)\times U(1)$ generators do not annihilate the vacuum and thus three of the four gauge bosons acquire masses. Linear combinations of these generators correspond to the $W^\pm$ and Z^0 gauge bosons. However, the vacuum remains invariant under the action of the Q operator, and $SU(2)_W \times U(1)_Y$ is spontaneously broken down to $U(1)_{\text{QED}}$. The electric charge is conserved and the physical photon remains massless.

3.5 Yukawa coupling

Yukawa interaction is the interaction between a scalar field ϕ and Dirac field Ψ. It was originally invented to describe the strong nuclear force between nucleons which is mediated by pions. Yukawa couplings constants are free parameters in the Standard Model. The Yukawa interaction is responsible for giving masses to the fermions.

$$\mathcal{L}_{f-s} = -G_e[\bar{R}(\phi^\dagger L) + (\bar{L}\phi)R] \tag{3.23}$$

where G_e is an empirical constant that is independent of the gauge couplings, g and $\frac{g'}{2}$. Substituting the reparameterised scalar field(3.17) and the Dirac fields(3.6) into the Yukawa term(3.23)

$$\mathcal{L}_{f-s} = -\frac{G_e\eta(x)}{\sqrt{2}}\bar{e}e - \frac{G_e v}{\sqrt{2}}\bar{e}e \tag{3.24}$$

The first term describes the interaction between the electron and the massive scalar field, η, while the second term contains the electron mass

$$m_e = \frac{G_e v}{\sqrt{2}} \tag{3.25}$$

The Yukawa interaction couples a left-handed multiplet to a right-handed multiplet. Right-handed neutrinos are not observed in nature and hence it will be hard to justify the introduction of a multiplet with right-handed neutrinos. Neutrinos cannot participate in the Yukawa interaction and they remain massless, for now.

3.6 Anomalies and Renormalisability

It is important to check that a gauge theory is renormalisable, that there is a way to consistently isolate and remove the infinities that crop up in the calculation of physical quantities such as the cross-section of a scattering process. Gerard't Hooft and Veltman showed in 1972 that the GSW theory is renormalisable, but the theory with only leptons contains anomalies which render the theory unrenormalisable[22].

Anomalies are quantum mechanical symmetry breakings. Classically, Nöther's theorem ensures that there is local current conservation associated to each continuous gauge symmetry. This holds at tree-level but Gross and Jackiw showed in the same year that this is violated at loop-level[23]. The quantisation proccess necessarily breaks classical symmetry and this makes the theory unrenormalisable. An example of a Feynman diagram that produces an anomaly in four dimensions is shown in figure 3.1[24]

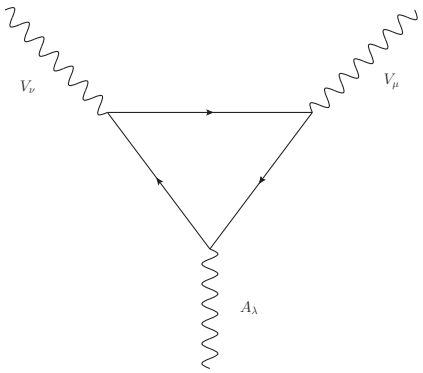

Figure 3.1: Triangle anomaly

Two vector and one axial current are coupled through the fermion loop and this leads to the breaking of chiral symmetry. Fortunately, this is the only fundamental anomaly and it vanishes when[23]

$$\Delta Q = Q_R - Q_L = 0 \tag{3.26}$$

where Q_R is the sum of the electric charges of the right-handed doublets and Q_L is the sum of electric charges of the left-handed doublets. There are three generations of leptons and quarks. Considering the first generation as an example,

$$Q_L^{\text{leptons}} = \begin{pmatrix} \nu_l \\ l^- \end{pmatrix}_L \qquad Q_L^{\text{quarks}} = \begin{pmatrix} u \\ d^c \end{pmatrix}_L \tag{3.27}$$

$$\begin{aligned} \Delta Q &= Q_L^{\text{leptons}} - Q_L^{\text{quarks}} \\ &= -1 + (\frac{2}{3} - \frac{1}{3}) = -\frac{2}{3} \neq 0 \end{aligned} \tag{3.28}$$

This shows that the GSW theory with only one lepton doublet and one quark double is not renormalisable. One can try to cancel the contributions from the left-handed doublets by introducing some right-handed doublets but right-handed weak doublets are not observed in nature. The alternative is to introduce more left-handed quark doublets.

$$\begin{pmatrix} u_{\text{red}} \\ d^c_{\text{red}} \end{pmatrix} \qquad \begin{pmatrix} u_{\text{blue}} \\ d^c_{\text{blue}} \end{pmatrix} \qquad \begin{pmatrix} u_{\text{green}} \\ d^c_{\text{green}} \end{pmatrix} \tag{3.29}$$

The introduction of these extra left-handed quark doublets cancel the anomaly and hence renormalisability of the weak interactions requires three internal degrees of freedom for the quarks.

3.7 Status of GSW theory

The GSW theory is based on a product group $SU(2)_W \times U(1)_Y$, leading to two independent coupling constants, g and $\frac{g'}{2}$, while a true unified theory should only have one coupling constant. Nevertheless, it partially unifies weak and electromagnetic interactions and is able to reproduce to QED and weak interaction phenomenology at the appropriate energy levels.

Another set-back of the theory is that fermion masses, various mixing angles and other physical quantities are free parameters in the theory which can only be constrained by experiments; a more fundamental theory is required to calculate these quantities. However, the theory is able to accurately predict the masses of $W^{\pm}$ and Z^0 once the weinberg mixing angle θ_W have been pinned down experimentally. The GSW theory has remarkable predictive power as it also predicted the existence and properties of the weak neutral current that is mediated by Z^0_μ, along with the existence of the charmed quark and Higgs boson.

The GSW theory is also consistent with other gauge theories like QCD. The renormalisability of GSW requires the quarks to have three internal degrees of freedom, which can then be interpreted as the color charges in QCD.

Chapter 4

Neutrino Physics

The neutrino started out as a book-keeping particle to save the conservation of energy. In 1911, Lise Meitner and Otto Hahn discovered that the electrons from β-decays had a continuous spectrum of energies. This finding was an apparent violation of energy conservation as nuclear decays were thought to be two-body problems, and so discrete emitted electron energies were expected. Further experiments confirmed this finding and the neutrino was thus theorised in 1930 by Pauli to account for the missing momentum and energy. An experiment to detect neutrinos was proposed in 1942 by Wang and the elusive particle was finally detected in 1956 by Cowan et al.[25][26]. This discovery was awarded the Physics Nobel Prize in 1995.

In the late 1960s, Davis and Bahcall found a deficit in the expected solar neutrino flux in the Homestake experiment. This was confirmed by data from the Kamiokande II detector in Japan in the 1980s[9]. This deficit then became known as the solar neutrino problem and it was eventually resolved by neutrino oscillations. Electron neutrinos from the sun oscillated during propagating into neutrinos of another flavour which the detectors was not sensitive to. The first experimental evidence of neutrino oscillation came from the Super-Kamiokande Collaboration in 1998[27]. Davis subsequently shared the 2002 Physics Nobel Prize with Masatoshi, who worked on the Kamiokande and Super-Kamiokande experiments. The very fact that neutrinos oscillate hints at the incompleteness of the Standard Model.

4.1 Massive neutrinos

Neutrinos are traditionally massless in the Standard Model. Fermions such as the charged leptons and quarks get their masses from their Yukawa couplings to the Higgs particle after the Electroweak spontaneous symmetry breaking. The neutrino remains massless due to the lack of right-handed neutrino which is required to construct the Yukawa coupling term. However, it is experimentally observed that neutrinos undergo oscillations, which implies that there is at least one massive neutrino[27].

The simplest way to construct mass terms for the neutrino is to introduce right-handed weak isosinglets, ν_R. These right-handed neutrinos are sterile and do not interact with other Standard Model particles, except via gravitation. Consequently, there are two possible types of neutrino mass terms - the Dirac mass term and the Majorana mass term. Note that having a Dirac mass term does not necessarily imply that the neutrino is a Dirac spinor. The name of the mass term simply refers to the structure of the mass term in the Lagrangian.

4.1.1 Dirac mass

The Dirac neutrino mass is built out of the left-handed neutrino and its sterile right-handed counterpart.

$$\mathcal{L}_{\text{Dirac}} = -\overline{\nu_R} m_D \nu_L + h.c. \tag{4.1}$$

where

$$\nu_L = \begin{pmatrix} \nu_{eL} \\ \nu_{\mu L} \\ \nu_{\tau L} \\ \vdots \end{pmatrix} \qquad \nu_R = \begin{pmatrix} \nu_{eR} \\ \nu_{\mu R} \\ \nu_{\tau R} \\ \vdots \end{pmatrix} \tag{4.2}$$

ν_L contains all the left-handed neutrino fields while ν_R contains the sterile right-handed fields. In this basis, m_D is a complex non-diagonal matrix. The Dirac mass term, along with the rest of the SM lagrangian, are invariant under a global guage transformation.

$$\nu_L \to e^{i\alpha}\nu_L \qquad \nu_R \to e^{i\alpha}\nu_R \qquad l \to e^{i\alpha} l \tag{4.3}$$

This symmetry implies that the total lepton number is conserved.

4.1.2 Majorana mass

The Majorana mass is constructed out of a neutrino field and its charge-conjugate.

$$\mathcal{L}_{\text{Maj.}} = -\frac{1}{2}\left(\overline{\nu_L^c} m_L \nu_L + \overline{\nu_R^c} m_R \nu_R\right) + h.c. \tag{4.4}$$

where ν_L^c is the charge-conjugate of ν_L. C is the unitary matrix of charge conjugation which statisfies

$$\nu_L^c = C\overline{\nu_L}^T \tag{4.5}$$

$$C\gamma_\alpha^T C^{-1} = -\gamma_\alpha \qquad C^T = -C \tag{4.6}$$

The Majorana mass term mixes particle and antiparticle and violates lepton number conservation. Therefore, such mass terms are only allowed if the neutrino does not carry other charges that are conserved by symmetry.

In general, the neutrino can have both Dirac and Majorana masses.

$$\begin{aligned}\mathcal{L}_{\text{mass}} &= -\overline{\nu_R} m_D \nu_L - \frac{1}{2}\left(\overline{\nu_L^c} m_L \nu_L + \overline{\nu_R^c} m_R \nu_R\right) + h.c. \\ &= \frac{1}{2}\overline{\Psi_L^c}\mathcal{M}\Psi_L + h.c\end{aligned} \tag{4.7}$$

where

$$\Psi_L = \begin{pmatrix}\nu_L^c \\ \nu_R\end{pmatrix} \qquad \mathcal{M} = \begin{pmatrix}m_L & m_D \\ m_D & m_R\end{pmatrix} \tag{4.8}$$

Compared to even the lightest charged lepton, neutrinos are extremely light. The strongest limit on neutrino masses comes from cosmology. The most recent data from the Planck collaboration sets an upperbound of 0.66 eV to the summed masses of the three neutrino species while the three year data from the WMAP collaboration sets a stronger upperbound of 0.3eV[28][29]. Looking at equation 4.7, there is no reason why the electron should be $\sim 10^6$ times heaver than the neutrinos. This disparity in masses can be explained by the See-saw mechanism.

4.1.3 See-saw mechanism

There are other types of see-saw mechanism which involve the addition of more exotic fields such as scalar $SU(2)_L$ triplets for type II see-saw mechanism and fermion triplets for type III see-saw mechanism[30][31]. For succinctness, only type I see-saw mechanism, which involves right-handed neutrino singlets, will be discussed. For simplicity, only one generation of leptons will be considered

Recall that the neutrino can have both Dirac and Majorana masses, expressed as equation 4.7. It will be more convenient to work in a basis in which the mass matrix, $\mathcal{M}$, is diagonal.

$$\mathcal{L}_{\text{mass}} = \frac{1}{2}\overline{\Psi_L'^c}\widetilde{\mathcal{M}}\Psi_L'^c + h.c \tag{4.9}$$

where

$$\Psi_L'^c = \begin{pmatrix}\nu \\ N\end{pmatrix} \qquad \widetilde{\mathcal{M}} = \begin{pmatrix}m_\nu & 0 \\ 0 & M\end{pmatrix} \tag{4.10}$$

The masses of the neutrinos, m_ν and M, are the eigenvalues of $\mathcal{M}$ and can be read off the diagonals of $\widetilde{\mathcal{M}}$. ν and N are the mass eigenstates of the neutrinos.

Solving for the eigenvalues of $\mathcal{M}$

$$\begin{vmatrix}m_L - \lambda & m_D \\ m_D & m_R - \lambda\end{vmatrix} = 0 \tag{4.11}$$

$$\lambda_\pm = \frac{1}{2}(m_L + m_R) \pm \frac{1}{2}\sqrt{(m_R + m_L)^2 - 4(m_L m_R - m_D^2)} \tag{4.12}$$

The Dirac mass term is a result of Yukawa couplings of the leptons to the Higgs after Electroweak spontaneous symmetry breaking and so it is justified to assume that m_D is of the order of the Electroweak scale, $m_D \sim 250$ GeV. The right-handed sterile neutrino was created when the universe was still at the GUT scale and hence m_R is often assumed to be at the GUT scale, $m_R \sim 10^{15}$ GeV. This results in a mass hierachy $M_{\text{GUT}} \simeq m_R >> m_D > m_L \simeq 0$. With these assumptions about the mass scales,

$$\begin{aligned} \lambda_- \equiv m_\nu &\simeq \frac{1}{2}m_R - \frac{1}{2}\sqrt{m_R^2 + 4m_D^2} \sim \frac{m_D^2}{m_R} \sim 0.06 \text{ GeV} \\ \lambda_+ \equiv M &\simeq \frac{1}{2}m_R + \frac{1}{2}\sqrt{m_R^2 + 4m_D^2} \sim m_R \sim 10^{15} \text{ GeV} \end{aligned} \tag{4.13}$$

The see-saw mechanism gives reasonably physical estimates of the neutrino masses and this only requires simple assumptions of the energy scale at which the active and sterile neutrinos were created.

4.2 Neutrino Oscillations

Proposed in 1957 by Pontecorvo, neutrino oscillation is a quantum mechanical phenomenon that is analogous to $K^0 - \overline{K^0}$ oscillations[32]. These oscillations are generated by the interference of the different mass eigenstates, which are detected coherently as they cannot be distinguished from each other due to the small mass differences. Neutrino oscillations experiments can shed light on fundamental questions such as whether CPT is really an exact symmetry, and provide an avenue for searching for physics beyond the Standard Model.

4.2.1 Plane-wave derivation

An important assumption necessary for the plane-wave derivation of neutrino oscillation probability is that the neutrinos are ultra-relativistic. This is a justified assumption as the neutrino mass is on the order of 1 eV while only neutrinos with energies larger than 100 keV can be detected[33].

Assuming there are n neutrino flavours, the n orthonormal flavour eigenstates $|\nu_\alpha\rangle$ are related to the n orthonormal mass eigenstates $|\nu_i\rangle$ via a unitary mixing matrix U

$$|\nu_\alpha\rangle = \sum_i U_{\alpha i} |\nu_i\rangle \qquad\qquad |\nu_i\rangle = \sum_\alpha U^*_{\alpha i} |\nu_\alpha\rangle \tag{4.14}$$

where

$$U^\dagger U = U U^\dagger = 1 \qquad\qquad \langle \nu_\beta | \nu_\alpha \rangle = \delta_{\alpha\beta} \qquad\qquad \langle \nu_i | \nu_j \rangle = \delta_{ij} \tag{4.15}$$

Only the relative phases are meaningful in quantum mechanics. With n orthogonal neutrino states, there are $n-1$ relative phases and hence $(n-1)^2$ free parameters, which

can be repackaged as mixing angles and CP-violating phases. It is then convenient to reparameterise the unitary mixing matrix U as an n-dimensional rotational matrix with ${}^{n}\mathrm{C}_2 = \frac{1}{2}n(n-1)$ weak mixing angles and $\frac{1}{2}(n-1)(n-2)$ CP-violating phases.

Solving the time dependent Schrödinger's equation, where $\hat{H}$ is the Hamiltonian of the system,

$$\hat{H}\left|\nu_i\right\rangle = E_i\left|\nu_i\right\rangle \tag{4.16}$$

the time evolution of the mass eigenstates can be expressed as plane waves

$$\left|\nu_i(x,t)\right\rangle = e^{-iE_it}\left|\nu_i(x,0)\right\rangle \tag{4.17}$$

where $\left|\nu_i(x,0)\right\rangle$ is the neutrino state at $t=0$. For neutrinos emitted with momentum p at position $\mathbf{x}=\mathbf{0}$ and time $t=0$,

$$\begin{aligned}\left|\nu_i(x,0)\right\rangle &= e^{i\mathbf{p}.\mathbf{x}}\left|\nu_i\right\rangle \\ \left|\nu_i\right\rangle &\equiv \left|\nu_i(0,0)\right\rangle\end{aligned} \tag{4.18}$$

For ultra-relativistic neutrinos,

$$E_i = \sqrt{m_i^2 + p_i^2} \simeq E + \frac{m_i^2}{2E} \tag{4.19}$$

The neutrinos are produced and detected via the weak force which couples to the flavour eigenstates. However, they propagate as mass eigenstates in between production and detection. If the difference in mass between two neutrino states with different masses cannot be resolved, the flavour neutrino will be a coherent superposition of the mass eigenstates. Neutrinos produced as a particular flavour $\left|\nu_\alpha\right\rangle$ at $t=0$ will evolve into a superposition of other flavours.

$$\begin{aligned}\left|\nu(x,t)\right\rangle &= \sum_i U_{\alpha i}\left|\nu_i(x,t)\right\rangle \\ &= \sum_{i,\beta} U_{\alpha i}e^{i(\mathbf{p}.\mathbf{x}-E_it)}\left|\nu_i\right\rangle \\ &= \sum_{i,\beta} U_{\alpha i}U^*_{\beta i}e^{i(\mathbf{p}.\mathbf{x}-E_it)}\left|\nu_\beta\right\rangle\end{aligned} \tag{4.20}$$

The time-dependent transition amplitude for a flavour conversion $\alpha \to \beta$ is then

$$A(\nu_\alpha \to \nu_\beta)(t) = \left\langle\nu_\beta|\nu(x,t)\right\rangle = \sum_i U_{\alpha i}U^*_{\beta i}e^{i(\mathbf{p}.\mathbf{x}-E_it)} \tag{4.21}$$

Substituting the condition for relativistic neutrinos in equation 4.19,

$$\begin{aligned}A(\nu_\alpha \to \nu_\beta)(t) &= \sum_i U_{\alpha i}U^*_{\beta i}\exp\left(-i\frac{m_i^2L}{2E}\right) \\ &= A(\nu_\alpha \to \nu_\beta)(L)\end{aligned} \tag{4.22}$$

where $L = x = ct$ is the distance between the source and the detector.

The transition probability is then

$$\begin{aligned} P(\nu_\alpha \to \nu_\beta)(t) = |A(\nu_\alpha \to \nu_\beta)|^2 &= \sum_{ij} U_{\alpha i} U^*_{\alpha j} U^*_{\beta i} U_{\beta j} e^{-i(E_i - E_j)t} \\ &= \sum_i |U_{\alpha i}|^2 |U^*_{\beta i}|^2 + 2\mathrm{Re} \sum_{j>i} U_{\alpha i} U^*_{\alpha j} U^*_{\beta i} U_{\beta j} \exp\left(-i \frac{\Delta m^2_{ij} L}{2E}\right) \\ &= \delta_{\alpha\beta} - 4 \sum_{j>i} \mathrm{Re}\left[U_{\alpha i} U^*_{\alpha j} U^*_{\beta i} U_{\beta j}\right] \sin^2\left(\frac{\Delta m^2_{ij} L}{4E}\right) \\ &+ 2 \sum_{j>i} \mathrm{Im}\left[U_{\alpha i} U^*_{\alpha j} U^*_{\beta i} U_{\beta j}\right] \sin\left(\frac{\Delta m^2_{ij} L}{2E}\right) \end{aligned} \tag{4.23}$$

where

$$\Delta m^2_{ij} = m^2_i - m^2_j \tag{4.24}$$

The first term in equation 4.23 is the average transition probability,

$$\left\langle P_{\nu_\alpha \to \nu_\beta} \right\rangle = \sum_i |U_{\alpha i}|^2 |U^*_{\beta i}|^2 = \sum_i |U_{\alpha i}|^2 |U^*_{\beta i}|^2 = \left\langle P_{\nu_\beta \to \nu_\alpha} \right\rangle \tag{4.25}$$

The second term in equation 4.23 describes the time and spatial dependence of the neutrino oscillations. In particular, if CP is conserved, $U_{\alpha i}$ is purely real and equation 4.23 is simplified to

$$\begin{aligned} P(\nu_\alpha \to \nu_\beta)(t) &= \delta_{\alpha\beta} - 4 \sum_{j>i} U_{\alpha i} U_{\alpha j} U_{\beta i} U_{\beta j} \sin^2\left(\frac{\Delta m^2_{ij} L}{4E}\right) \\ &= \delta_{\alpha\beta} + \sum_{j>i} U_{\alpha i} U_{\alpha j} U_{\beta i} U_{\beta j} \cos\left(2\pi \frac{x}{L_{osc.}}\right) \end{aligned} \tag{4.26}$$

The transition probability has an oscillatory behaviour which is a function of the distance travelled, x. It can also be expressed in terms of the oscillation length, $L_{osc.}$, between $|\nu_\alpha\rangle$ and $|\nu_\beta\rangle$.

$$\begin{aligned} \frac{\Delta m^2_{ij} L}{2E} &\equiv 2\pi \frac{x}{L_{osc.}} \\ L_{osc.} &= 2\pi \frac{2p_\nu}{\Delta m^2_{ij}} \end{aligned} \tag{4.27}$$

where p_ν is the momentum of the neutrino. $L_{osc.}$ can be interpreted as the distance at which the phase generated by Δm^2_{ij} becomes equal to 2π.

4.2.2 Comments on neutrino oscillation probabilities

If the neutrinos are measured very near the source, $x << L_{osc.}$, most of the neutrinos will be measured in their original flavour. Conversely, if the neutrinos are measured very far away from the source, $x >> L_{osc.}$, the oscillation pattern will be washed out. This is due

to the spread in momentum Δp_ν in the neutrino beam. If a neutrino in the beam with momentum p_ν has a phase shift of $\sim \pi$ with respect to another neutrino in the beam with momentum $p'_\nu = p_\nu + \frac{\Delta p_\nu}{2}$, the oscillation will be cancelled out on average. In this scenario, it is still possible to detect a neutrino of a different flavour from its original flavour but the probability will no longer vary with distance.

From equation 4.26, one infers that oscillation requires non-trivial mixing and at least one specie of neutrinos to have mass. The oscillatory behaviour arises from the interference between the different mass eigenstates in the neutrino wavefunction. It is governed by the second term which vanishes if the neutrinos have equal masses, $\Delta m^2_{ij} = 0$. The oscillatory term will also vanish if there is no mixing between amongst the different flavours and there are no non-trivial off-diagonal elements in U. At macroscopic distances, this effect of flavour oscillation can be large despite the small differences in neutrino masses, Δm^2_{ij}.

Note also that the oscillation probability in equation 4.23 depends on the elements of the mixing matrix U through the quartic product,

$$U_{\alpha i} U^*_{\alpha j} U_{\beta i} U^*_{\beta j} \tag{4.28}$$

which is invariant under the phase transformation

$$U_{\alpha j} \to e^{i\phi_\alpha} U_{\alpha j} e^{\phi_j} \tag{4.29}$$

This corresponds to giving a phase to the charged lepton and neutrino fields. In fact, the quartic product in equation 4.28 is free from the Majorana phases and hence they cannot be measured in neutrino oscillation experiments[33].

4.2.3 Antineutrino transition probability

The unitary mixing matrix relating the neutrino flavour and mass eigenstates in equation 4.14 is associated to the unitary matrix relating the antineutrino flavour and mass eigenstates by complex conjugation.

$$|\overline{\nu_\alpha}\rangle = \sum_i U^*_{\alpha i} |\overline{\nu_i}\rangle \qquad\qquad |\overline{\nu_i}\rangle = \sum_\alpha U_{\alpha i} |\overline{\nu_\alpha}\rangle \tag{4.30}$$

Since massive neutrinos and antineutrinos share the same the kinematical properties, the derivation for the antineutrino transition probability follows the same lines as the derivation for neutrino transition probability and the following result is obtained.

$$\begin{aligned} P(\overline{\nu_\alpha} \to \overline{\nu_\beta})(t) = \delta_{\alpha\beta} - 4 \sum_{j>i} \mathrm{Re}\left[U_{\alpha i} U^*_{\alpha j} U^*_{\beta i} U_{\beta j}\right] \sin^2\left(\frac{\Delta m^2_{ij} L}{4E}\right) \\ - 2 \sum_{j>i} \mathrm{Im}\left[U_{\alpha i} U^*_{\alpha j} U^*_{\beta i} U_{\beta j}\right] \sin\left(\frac{\Delta m^2_{ij} L}{2E}\right) \end{aligned} \tag{4.31}$$

The only difference is the sign of the imaginary part of the mixing matrix elements.

4.2.4 Types of neutrino oscillation experiments

Neutrino oscillations experiments can be categorised according to the type of neutrinos utilised and the distance between the neutrino source and the detector. The type of neutrino source will determine the energy of the neutrinos observed in the experiment. The ratio between the source-detector distance and the neutrino energy then determines the experiment's sensitivity to Δm^2_{ij}.

To understand how the Δm^2_{ij} sensitivity is affected by the neutrino energy and source-detector distance, one has to examine the oscillation phase in equation 4.26.

$$\frac{\Delta m^2_{ij} L}{2E} = 2.53 \times \left(\frac{\Delta m^2_{ij}}{1\text{eV}^2}\right) \times \left(\frac{1\text{MeV}}{E}\right) \times \left(\frac{L}{1\text{m}}\right) \tag{4.32}$$

This oscillation phase can also be expressed in terms of the oscillation length, $L_{osc.}$

$$L_{osc.} = 2.48\text{m} \times \left(\frac{E}{1\text{MeV}}\right) \times \left(\frac{1\text{eV}^2}{\Delta m^2_{ij}}\right) \tag{4.33}$$

To observe neutrino oscillations, the oscillation phase in equation 4.32 must be of order one. The sensitivity to Δm^2_{ij} of a neutrino oscillation experiment is then dependent on the characteristic ratio L/E that is determined by the experimental setup. Using longer baselines or smaller energies moves the sensitivity to smaller Δm^2_{ij}. Short baseline (SBL) experiments are defined to have sensitivity $\Delta m^2_{ij} \gtrsim 0.1\text{eV}^2$ while long baseline (LBL) experiments have sensitivity $\Delta m^2_{ij} < 0.1\text{eV}^2$.

Experiment type	**L**	**E**	$\mathbf{\Delta m^2_{ij}}$ **sensitivity**	**Examples**
Reactor SBL	~ 10 m	~ 1 MeV	~ 0.1 eV^2	Gosgen[34], Rovno[35]
Accelerator SBL (Pion decay in flight)	~ 1 km	$\gtrsim 1$ GeV	$\gtrsim 1$ eV^2	NOMAD[36], CHORUS[37]
Accelerator SBL (Muon decay at rest)	~ 10 m	~ 10 MeV	~ 1 eV^2	KARMEN[38], LSND[39]
Accelerator SBL (Beam Dump)	~ 1 km	$\sim 10^2$ GeV	$\sim 10^2$ eV^2	CHARM[40]
Reactor LBL	~ 1 km	~ 1 MeV	$\sim 10^{-3}$ eV^2	CHOOZ[41], Palo Verde[42]
Accelerator LBL	$\sim 10^3$ km	$\gtrsim 1$ GeV	$\gtrsim 10^{-3}$ eV^2	T2K[43], MINOS[44]
Atmospheric	$20 - 10^4$ km	$0.5 - 10^2$ GeV	$\sim 10^{-4}$ eV^2	Super-Kamiokande[45], Soudan-2[46]
Solar	$\sim 10^{11}$ km	$0.2 - 15$ MeV	$\sim 10^{-12}$ eV^2	Homestake[47], SNO[48]

Table 4.1: Types of neutrino oscillation experiments with their typical sensitivity to Δm^2_{ij}

Short baseline experiments are divided according to their neutrino source into reactor SBL and accelerator SBL experiments. Reactor SBL experiments utilize large isotropic fluxes of electron antineutrinos produced in β^--decays of heavy nuclei such as ^{235}U, ^{238}U and ^{239}Pu. Accelerator SBL experiments use beams of neutrinos from the decay of particles, such as pions, kaons and musons, created by a proton beam hitting a target. The distance between the source and detector in SBL experiments are typically not more than 1 km. Long baseline experiments have similar sources to SBL experiments but the distance between the source and detector are two to three orders of magnitude longer.

It is also possible to use natural neutrino sources in experiments. Primary cosmic rays interact with the upper layers of the atmosphere, producing pions and kaons which then decay into muons (which subsequently decay into more neutrinos) and neutrinos. Atmospheric neutrino experiments detect these neutrinos which have a wide range of energies from 500 MeV to 100 GeV. The distance between the source and the detector also has a wide range from ~ 20 km for neutrinos coming from overhead to $\sim 1.3 \times 10^4$ km for neutrinos coming from the other side of Earth. This makes atmospheric neutrino experiments sensitive to very small mass differences.

Another natural neutrino source would be the Sun. Solar neutrino experiments detect the neutrinos generated by the thermonuclear reactions in the core of the Sun. The distance between the Sun and Earth is $\sim 1.5 \times 10^8$ km and the solar neutrinos have energies in the range $0.2 - 15$ MeV. This makes solar neutrino experiments sensitive to Δm^2_{ij} much smaller than the other types of neutrino oscillation experiments. A table of the various types of experiments along with their Δm^2_{ij} sensitivies are summarised in table 4.1.

4.2.5 Appearance vs Disappearance experiments

Neutrino oscillation experiments are divided into appearance experiments and disappearance experiments. Appearance experiments measure the transition probability by searching for neutrinos of a different flavour to the incoming neutrino beam. Hence there is little contamination from the incoming beam and these such experiments can be sensitive to very small mixing angles. Disappearance experiments measure the survival probability by counting the number of interactions in the detector and comparing it with the expected one. The number of expected and detected events have statistical fluctuations, making it difficult to measure small values of mixing angle.

4.2.6 Pontecorvo-Maki-Nakagawa-Sakata(PMNS) matrix

When the mixing between the three neutrino species is considered, equation 4.14 becomes

$$\begin{pmatrix} \nu_e \\ \nu_\mu \\ \nu_\tau \end{pmatrix} = U \begin{pmatrix} \nu_1 \\ \nu_2 \\ \nu_3 \end{pmatrix} \tag{4.34}$$

where U is the Pontecorvo-Maki-Nakagawa-Sakata(PMNS) matrix which is commonly parameterised in equation 4.35. The PMNS matrix describes a rotation between the mass and flavour basis, with the rotation characterised by the three mixing angles, $\theta_{12}, \theta_{13}, \theta_{23}$. CP violation in the lepton sector is characterised by the phase, δ, and it is just convention to put it in the term with θ_{13}. α, β are Majorana phases which are only relevant if neutrinos are Majorana particles. These phases are not observable in oscillation experiments.

$$
\begin{aligned}
U &= \begin{pmatrix} U_{e1} & U_{e2} & U_{e3} \\ U_{\mu 1} & U_{\mu 2} & U_{\mu 3} \\ U_{\tau 1} & U_{\tau 2} & U_{\tau 3} \end{pmatrix} \\
&= \underbrace{\begin{pmatrix} 1 & 0 & 0 \\ 0 & \cos\theta_{23} & \sin\theta_{23} \\ 0 & -\sin\theta_{23} & \cos\theta_{23} \end{pmatrix}}_{\text{Atmospheric}} \underbrace{\begin{pmatrix} \cos\theta_{13} & 0 & \sin\theta_{13}e^{i\delta} \\ 0 & 1 & 0 \\ -\sin\theta_{13}e^{i\delta} & 0 & \cos\theta_{13} \end{pmatrix}}_{\text{Cross-mixing}} \underbrace{\begin{pmatrix} \cos\theta_{12} & \sin\theta_{12} & 0 \\ -\sin\theta_{12} & \cos\theta_{12} & 0 \\ 0 & 0 & 1 \end{pmatrix}}_{\text{Solar}} \underbrace{\begin{pmatrix} e^{i\alpha/2} & 0 & 0 \\ 0 & e^{i\beta/2} & 0 \\ 0 & 0 & 1 \end{pmatrix}}_{\text{Majorana phases}}
\end{aligned}
\tag{4.35}
$$

Under this parameterisation, the PMNS matrix factorises into three terms, with each of the terms corresponding to a different experimental regime. The first term in equation 4.35 is identified with atmospheric neutrino mixing and is driven by a large mass difference of $|\Delta m^2_{atm.}| = 2.43 \times 10^{-3}\text{eV}^2$. Atmospheric neutrino and accelerator LBL experiments are sensitive to mass splittings of this magnitude and the mixing angle is measured to be $\sin^2(2\theta_{23}) > 0.95(90\%\text{C.L})$.

The second term is related to the cross-mixing of the first and third mass eigenstates. The CP violating phase, δ, are currently unknown but the mixing angle has been measured to be $\sin^2(2\theta_{13}) = 0.095 \pm 0.010$. Experiments that are sensitive to this term are usually accelerator LBL experiments, such as T2K and MINOS, and reactor SBL experiments such as Daya Bay. Experiments that are sensitive to θ_{13} and have access to both neutrino and antineutrinos, such as T2K, are capable of measuring the CP violating phase, δ_{CP}. It will be interesting to know if δ in the leptonic sector is enough to account for matter antimatter asymmetry in the universe.

The third term is associated with solar neutrino mixing and is driven by a relatively small mass splitting of $\Delta m^2_{Solar} \equiv \Delta m^2_{21} = (7.5 \pm 0.2) \times 10^{-5}\text{eV}^2$. Measurements in this regime are usually made by solar neutrino experiments and θ_{13} is measured to be $\sin^2(2\theta_{12}) = 0.857 \pm 0.024$ [49].

4.3 Open questions

Oscillation experiments have shed light on the three mixing angles and the absolute values of the mass differences. However, little is known about the nature (whether it is a Dirac or Majorana particle) and about the absolute masses of the neutrinos. These two properties of the neutrino can be probed by experiments (e.g. Heidelberg-Moscow experiment) that are searching for neutrinoless double β-decays[50].

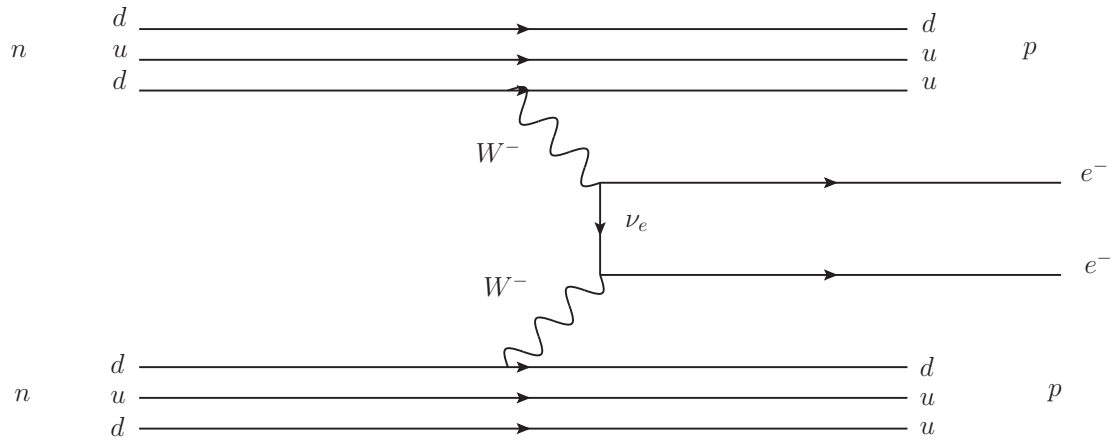

Figure 4.1: Neutrinoless double β-decay

Observations of such decays will imply that neutrinos are Majorana particles. The mass of the neutrino can be measured from β-decay spectrums. The KATRIN experiment is designed to measure the mass of the electron antineutrino with sub-eV precision by analysing the high-energy tail of nuclear β-decays of Tritium[51].

The number of neutrino species is measured to be $N_\nu = 3.00 \pm 0.08$ from the decay widths of the Z-boson[52]. This means that the 3×3 PMNS matrix holds complete information about neutrino mixing and is unitary.

$$\begin{aligned} |U_{l1}|^2 + |U_{l2}|^2 + |U_{l3}|^2 &= 1|_{l=e,\mu,\tau} \\ |U_{ei}|^2 + |U_{\mu i}|^2 + |U_{\tau i}|^2 &= 1|_{i=1,2,3} \\ U_{l1}U^*_{l'1} + U_{l2}U^*_{l'2} + U_{l3}U^*_{l'3} &= 0|_{l,l'=e,\mu,\tau;l\neq l'} \\ U_{ei}U^*_{ej} + U_{\mu i}U^*_{\mu j} + U_{\tau i}U^*_{\tau j} &= 0|_{i,j=1,2,3;i\neq j} \end{aligned} \tag{4.36}$$

However, it is possible to have a fourth neutrino specie that is so heavy that is it able to fit within the decay width of the Z-boson. In fact, results from the LSND experiment hints at the existence of a sterile fourth neutrino specie[53]. With the combination of solar neutrino experiments and SBL experiments such as, Daya Bay and JUNO, it is possible to test the unitarity of the PMNS matrix directly by checking that the conditions in 4.36 are satisfied[54].

Chapter 5

T2K experiment

The Tokai-to-Kamioka(T2K) experiment is a long baseline accelerator neutrino oscillation experiment. The intense ν_μ beam is produced at the Japanese Proton Accelerator Research Complex(J-PARC) in Tokai, and directed(2.5°off-axis) at the Super-Kamiokande(SK) water Cherenkov detector 295km away in Kamioka.

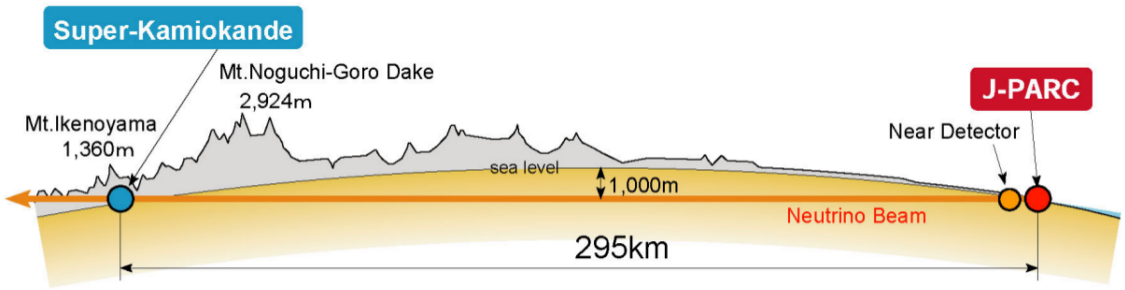

Figure 5.1: Schematic of the T2K experiment. The neutrinos travelled 295 km through the Earth from the J-PARC source to the Super-Kamiokande detector. Figure taken from [3]

At J-PARC, protons accelerated up to 30 GeV interact with a graphite target, producing a large number of secondary mesons. These mesons are then focussed by magnetic horns into a meson beam which travel through a decay volume where they decay and produce neutrinos. The ν_μ are primarily produced via the following processes

$$\pi^+ \to \mu^+ + \nu_\mu$$
$$K^+ \to \mu^+ + \nu_\mu$$

There is a small contamination ($\sim 1\%$) from $\overline{\nu}_\mu$ and ν_e via the following unwanted

processes[55]

$$K^+ \rightarrow \pi^0 + e^+ + \nu_e$$
$$\mu^+ \rightarrow e^+ + \nu_e + \overline{\nu}_\mu$$

The properties of the neutrino beam, such as the neutrino flux, energy spectrum and beam composition, are then measured at the ND280 near detector suite which is 280 m downstream of the graphic target. The ND280 detector suite consists of the INGRID on-axis detector and the ND280 detector which is collinear with the neutrino source and the SK far detector(2.5° off-axis).

The SK detector is a cylinder containing 50 kTons of pure water surrounded by $\sim 13,000$ photomultiplier tubes. The 36.2m high detector has a diameter of 33.8 m and sits in a cavern 1 km underground, 295 km away from the J-PARC facility. The large distance between the neutrino source and the SK detector allows sufficient time for the $\nu_\mu \rightarrow \nu_e$ oscillation to occur. The SK detector is 2.5% off-axis and this modifies the neutrino energy spectrum observed. The flux at higher neutrino energies is reduced while the flux at the energy optimal for observing ν_μ disappearance is increased. This results in a narrow band beam which reduces the expected background events, hence allowing the neutrino oscillation parameters and mass differences to be measured more accurately.

Currently, a ν_μ beam is used but it is possible to for J-PARC to produce $\overline{\nu}_\mu$ beams as well. Details on the instrumentation aspect of the T2K experiment can be found in [56].

5.1 Physics goals

The primary goal of T2K is to measure the oscillation of ν_μ to ν_e. Observations of such oscillations will imply that $\theta_{13} \neq 0$. It is then possible to measure the mixing angle, θ_{13}, via the transition probability

$$P(\nu_\mu \rightarrow \nu_e) = \sin^2\theta_{23}\sin^2(2\theta_{13})\sin^2\left(1.27\frac{\Delta m^2_{32}(eV^2)L(km)}{E(GeV)}\right) \tag{5.1}$$

T2K is also capable of making precise measurements of Δm^2_{23} and θ_{23}. This can be obtained from the ν_μ survival probability[57]

$$P(\nu_\mu \rightarrow \nu_\mu) = 1 - \sin^2(2\theta_{23})\sin^2\left(1.27\frac{\Delta m^2_{23}(eV^2)L(km)}{E(GeV)}\right) \tag{5.2}$$

The current limits on the atmospheric mixing parameters, $\sin^2(2\theta_{23})$ and $\Delta^2 m_{32}$ are currently set by MINOS, K2K and T2K but T2K will achieve sensitivities of $\delta(\Delta m^2_{32}) = 10^{-4}\text{eV}^2$ and $\delta(\sin^2(2\theta_{23})) = 0.01$[55].

By using a $\overline{\nu}_\mu$ beam and comparing differences in neutrino-antineutrino cross-sections, it is also possible to measure the CP-violating phase δ.

5.2 Neutrino detection

Neutrinos are detected at the SK detector via the charged-current quasi-elastic (CCQE) process. Lepton flavour is conserved at this level, hence the flavour of the incoming neutrino can be inferred from the flavour of the final-state charged lepton.

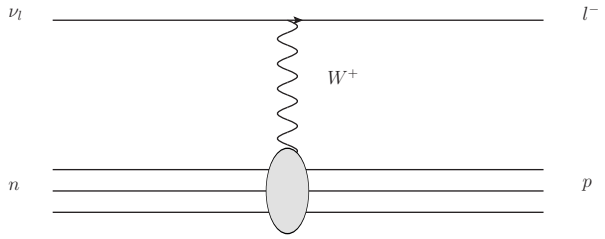

Figure 5.2: Tree-level charged-current quasi-elastic(CCQE) neutrino scattering

The T2K neutrino flux peaks at ~ 700 MeV. At this incoming neutrino energy, the outgoing charged leptons will have energies ~ 600 MeV, making them ultra-relativistic. These charged leptons will produce a cone of Cherenkov photons as they travel faster than the speed of light in water. The photons then produce a ring pattern when they hit the PMTs on the detector walls. An example of a muon-like event is shown in figure 5.3. Information about the interaction, such as the event vertex position and the momentum of the final state particles, can be extracted from the geometry of the Cherenkov ring.

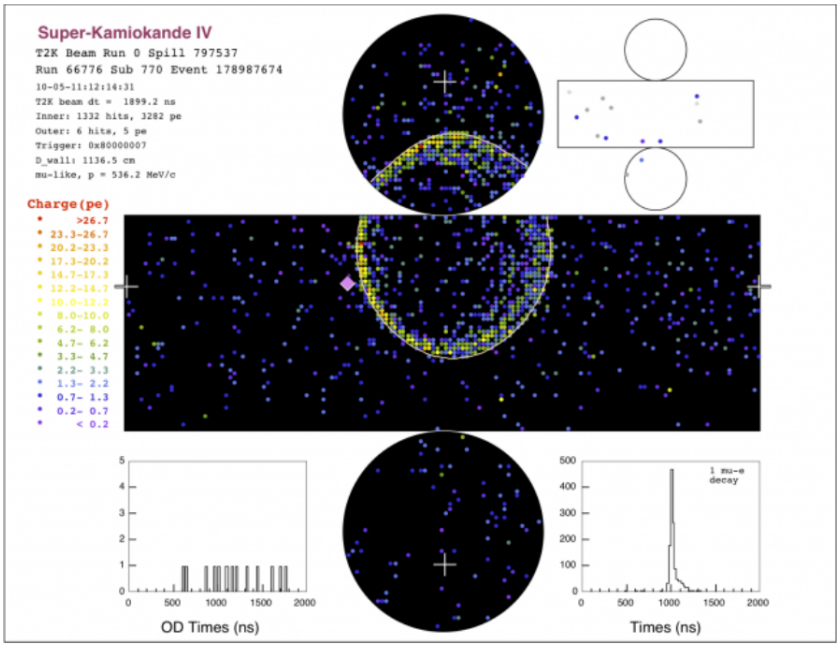

Figure 5.3: Example of a muon-like event detected at the SK detector. Image taken from [4]

To measure ν_μ disappearance, the number of muon-like events have to be counted at the SK detector. Muons are relatively massive and are miminum ionizing particles. They do not lose much energy as they travel through the SK detector, producing sharp Cherenkov ring images. On the other hand, electrons are light and experience multiple scattering between being produced at the neutrino interaction vertex and exiting the SK detector. The sum of the overlapping Cherenkov light cones result in a fuzzy ring detected by the PMTs. The SK event reconstruction software then uses the fuzziness of the ring to discern whether the image is more likely to be caused by muon-like or electron-like particles.

5.3 Neutrino interactions

5.3.1 Llewellyn-Smith formalism for neutrino-free nucleon scattering

The scattering proccesses that neutrinos and antineutrinos undergo with nucleons are

$$\begin{aligned} \nu_l + n &\to l^- + p \\ \bar{\nu}_l + p &\to l^+ + n \end{aligned} \tag{5.3}$$

The neutrino, corresponding charged lepton, initial nucleon and final nucleon have 4-momentum q_1, q_2, p_1, p_2 respectively. The neutrino is approximately massless, the charged lepton has mass m, while the nucleons have equal masses, M. The

4-momentuma are

$$\begin{aligned} q_1 &= \left(E_\nu, \boldsymbol{p_\nu}\right) \\ q_2 &= \left(E_l, \boldsymbol{p_l}\right) \\ p_1 &= \left(M, \mathbf{0}\right) \\ p_2 &= \left(E, \boldsymbol{p}\right) \end{aligned} \tag{5.4}$$

The general nucleon weak interaction current operator is defined as[58]

$$\langle p| J_\mu^+ |n\rangle = \cos\theta_c \left[\overline{p(p_2)}\Gamma_\mu n(p_1)\right] \tag{5.5}$$

where $\overline{p(p_2)}$ and $n(p_1)$ are the final and initial state of the nucleon respectively. The hadronic vertex, Γ_μ, is parameterised by two second class form factors(F_V^3, F_A^3) and four first class form factors — vector current form factors, F_1, F_2, axial vector form factor, F_A, and pseudo scalar form factor, F_P.

$$\Gamma_\mu = \gamma_\mu(F_1 + F_A\gamma_5) + \frac{1}{2M} i\sigma_{\mu\nu}q^\nu \xi F_2 + \frac{1}{M} P_\mu F_A^3\gamma_5 + \frac{q_\mu}{M}(F_V^3 + F_P\gamma_5) \tag{5.6}$$

where ξ is the difference between the relative anomalous magnetic moment of the interacting nucleons.

$$\xi = \kappa_p - \kappa_n = 3.706 \tag{5.7}$$

The form factors are functions of the momentum transfer, Q^2. For simplicity, they are assumed to adopt the dipole form even though recent precision electron scattering experiments reveal small deviations of the vector form factor from the simple dipole form [59].

$$F_1(Q^2) = \frac{1 + \frac{Q^2}{4M^2}(1+\xi)}{\left(1 + \frac{Q^2}{4M^2}\right)\left(1 + \frac{Q^2}{M_V^2}\right)^2} \tag{5.8}$$

$$F_2(Q^2) = \frac{\xi}{\left(1 + \frac{Q^2}{4M^2}\right)\left(1 + \frac{Q^2}{M_V^2}\right)^2} \tag{5.9}$$

$$F_A(Q^2) = \frac{g_A}{\left(1 + \frac{Q^2}{M_A^2}\right)^2} \qquad g_A = 1.267 \tag{5.10}$$

$$F_P(Q^2) = \frac{2M^2}{m_\pi^2 + Q^2} F_A(Q^2) \tag{5.11}$$

where M, m_π, M_A, M_V are the nucleon mass, pion mass, axial mass and vector mass respectively. The axial and vector masses are parameters that tune the dipole form of the axial and vector form factors. The vector form factors are measured in electron scattering experiments while the axial form factors are measured in neutrino scattering experiments. The vector and axial masses are then obtained by fitting the observed Q^2 distributions in scattering events.

An alternative way of parameterising the hadronic vertex is[60]

$$\Gamma_\mu = \gamma_\mu(g_V - g_A\gamma_5) - P_\mu(f_v - f_A\gamma_5) + q_\mu(h_V - h_A\gamma_5) \tag{5.12}$$

where $g_V, g_A, f_V, f_A, h_V, h_A$ are the familiar form factors in Fermi theory with the V-A structure as seen in section 2.4. The derivation of the differential cross-section will be carried out using the parameterisation in equation 5.12 for notational familiarity. However, for historical reasons, the code is written following the parameteristion in equation 5.6. It is possible to get from one parameterisation to the other by using the Gordon's decomposition.

$$\bar{u}(p')\gamma^{\mu}u(p) = \bar{u}(p')\left[\frac{(p'+p)^{\mu}}{2m} + \frac{i\sigma^{\mu\nu}(p'-p)_{\nu}}{2m}\right]u(p) \tag{5.13}$$

Using the Feynman rules, the differential cross-section is

$$\begin{aligned}\frac{d\sigma}{dQ^2} &= \frac{1}{64\pi E_{\nu}^2 M^2}\frac{G_F^2}{2(2s_p+1)(2s_{\nu}+1)} \\ &\times \sum_{spin}\left[\cos\theta_c(\bar{p}\Gamma_{\mu}n)\right]\left[\cos\theta_c(\bar{p}\Gamma_{\nu}n)\right]^{\dagger}\left[\bar{l}\gamma^{\mu}(1-\gamma_5)\nu\right]\left[\bar{l}\gamma^{\nu}(1-\gamma_5)\nu\right]^{\dagger} \\ &= \frac{1}{64\pi E_{\nu}^2 M^2}\frac{G_F^2\cos^2\theta_c}{4}\omega_{\mu\nu}\tau^{\mu\nu}\end{aligned} \tag{5.14}$$

The first term came from the Lorentz-invariant phase space while $\omega_{\mu\nu}$ and $\tau^{\mu\nu}$ are the tensors associated to the hadronic and leptonic legs respectively. G_F is Fermi's constant. Calculation of the charged-current tensors is straight-forward but non-trivially tedious, hence only a sketch of the calculation will be provided here. A merticulous derivation can be found in [57].

Proceeding with the leptonic tensor, $\tau_{\mu\nu}$, and using gamma matrix algebra(see appendix A.1),

$$\begin{aligned}\tau_{\mu\nu} &= Tr\left\{\left[\bar{l}\gamma_{\mu}(1-\gamma_5)\nu\right]\left[\bar{\nu}\gamma_{\nu}(1-\gamma_5)l\right]\right\} \\ &= 2Tr\left[\gamma_{\mu}\not{q}_1\gamma_{\nu}\not{q}_2\right] + 8i\epsilon_{\mu\alpha\nu\beta}q_{1\alpha}q_{2\beta} \\ &= 8[q_{1\mu}q_{2\nu} - (q_1\cdot q_2)g_{\mu\nu} + q_{2\mu}q_{1\nu}] + 8i\epsilon_{\mu\alpha\nu\beta}q_{1\alpha}q_{2\beta} \\ &= 4[n_{\mu}n_{\nu} - q_{\mu}q_{\nu} + (q^2-m^2)g_{\mu\nu} + i\epsilon_{\mu\nu\alpha\beta}n_{\alpha}q_{\beta}]\end{aligned} \tag{5.15}$$

where the antisymmetric property of $\epsilon_{\mu\alpha\nu\beta}$ and the following relation is used to get from the penultimate line to the last line.

$$n_{\mu}q_{\nu} = (q_1+q_2)_{\mu}(q_1-q_2)_{\nu} \tag{5.16}$$

Moving on to the hadronic tensor,

$$\begin{aligned}\omega_{\mu\nu} &= Tr\left\{\left[\bar{p}\{\gamma_{\mu}(g_V - g_A\gamma_5) - P_{\mu}(f_V - f_A\gamma_5) + q_{\mu}(h_V - h_A\gamma_5)\}n\right]\times\right. \\ &\quad \left.\left[\bar{n}\{\gamma_{\nu}(g_V^* - g_A^*\gamma_5) - P_{\nu}(f_V^* + f_A^*\gamma_5) + q_{\nu}(h_V^* + h_A^*\gamma_5)\}p\right]\right\} \\ &= \omega_1 g_{\mu\nu} + \omega_2 P_{\mu}P_{\nu} + \omega_3 i\epsilon_{\mu\nu\alpha\beta}q_{\alpha}P_{\beta} + \omega_4 q_{\mu}q_{\nu} + \omega_5(P_{\mu}q_{\nu} + P_{\nu}q_{\mu}) + \omega_6(P_{\mu}q_{\nu} - P_{\nu}q_{\mu})\end{aligned} \tag{5.17}$$

where

$$\begin{aligned}
\omega_1 &= -8M^2 g_A^2 + 2q^2(g_V^2 + g_A^2) \\
\omega_2 &= 2g_A^2 + 2|g_V - 2Mf_V|^2 - 2q^2(f_V^2 + f_A^2) \\
\omega_3 &= -4\mathrm{Re}[g_A^* g_V] \\
\omega_4 &= -2g_V^2 - 2|g_A + 2Mh_A|^2 + 2(-q^2 + 4M^2)(h_V^2 + h_A^2) \\
\omega_5 &= 4M\mathrm{Re}\left[\{g_V - 2Mf_V(1 - \frac{q^2}{4M^2})\}h_V^* + \{g_A^* + \frac{q^2}{2M}h_A^*\}f_A\right] \\
\omega_6 &= i4M\mathrm{Im}\left[\{g_V - 2Mf_V(1 - \frac{q^2}{4M^2})\}h_V^* + \{g_A^* + \frac{q^2}{2M}h_A^*\}f_A\right]
\end{aligned} \tag{5.18}$$

Substituting the hadronic and leptonic tensors back into equation 5.14, the neutrino-nucleon differential cross-section is

$$\frac{d\sigma}{dQ^2}\begin{pmatrix}\nu_l + n \to l^- + p \\ \bar{\nu}_l + p \to l^+ + n\end{pmatrix} = \frac{M^2 G_F^2 \cos^2\theta_c}{8\pi E_\nu^2}\left[A(Q^2) \pm B(Q^2)\frac{(s-u)}{M^2} + C(Q^2)\frac{(s-u)^2}{M^4}\right] \tag{5.19}$$

where s and u are the Mandelstam variables. For an event in which an ingoing neutrino of energy E_ν scatters of a nucleon of mass M with momentum transfer, Q^2, and producing an outgoing charged lepton of mass m,

$$(s-u) = 4ME_\nu - Q^2 - m^2 \tag{5.20}$$

$A(Q^2), B(Q^2), C(Q^2)$ are functions of the form factors given as

$$\begin{aligned}
A(Q^2) = \frac{(m^2+Q^2)}{M^2}\Bigg\{ & \left(1 + \frac{Q^2}{4M^2}\right)|F_A|^2 - \left(1 - \frac{Q^2}{4M^2}\right)|F_1|^2 \\
& \frac{Q^2}{4M^2}\left(1 - \frac{Q^2}{4M^2}\right)|\xi F_2|^2 + \frac{Q^2}{M^2}\mathrm{Re}(F_1^*\xi F_2) - \frac{Q^2}{M^2}\left(1 + \frac{Q^2}{4M^2}\right)|F_A^3|^2 \\
& - \frac{m^2}{4M^2}\left[|F_1 + \xi F_2|^2 + |F_A + 2F_P|^2 - 4\left(1 + \frac{Q^2}{4M^2}\right)\left(|F_V^3|^2 + |F_P|^2\right)\right]\Bigg\} \\
B(Q^2) = \frac{Q^2}{M^2}\mathrm{Re}\left[F_A^*(F_1 + \xi F_2)\right] - \frac{m^2}{M^2}\mathrm{Re}\left[\left(F_1 - \frac{Q^2}{4M^2}\xi F_2\right)F_V^{3*} - (F_A^* - \frac{Q^2}{2M^2}F_P)F_A^3\right] \\
C(Q^2) = \frac{1}{4}\left[|F_A|^2 + |F_1|^2 + \frac{Q^2}{4M^2}|\xi F_2|^2 + \frac{Q^2}{M^2}|F_A^3|^2\right]
\end{aligned} \tag{5.21}$$

The double differential cross-section for antineutrinos is obtained by crossing symmetry and replacing $q_2 \leftrightarrow -q_1$ which corresponds to $s \leftrightarrow u$. This results in the following exchange

$$\begin{aligned}
\frac{d\sigma}{dQ^2}(s,t,u) &\to \frac{d\sigma}{dQ^2}(u,t,s) \\
B(Q^2) &\to -B(Q^2)
\end{aligned}$$

The second class form factors, F_V^3 and F_A^3, violate G-parity and do not exist in the Standard Model[61]. These terms are therefore not included in the simulation.

5.4 Nuclear environment

In high energy processes $\mathcal{O}(100$ GeV), such as neutrino deep inelastic scattering, the neutrinos interact with leptons and asymptotically free partons. In this energy regime, perturbative QCD is applicable and the nuclear effects are not significant. However, at neutrino energies relevant to the SK detector ($E_\nu < 30$GeV), the neutrinos interact with bound nucleons and the nuclear environment of the nucleus has to be taken into account.

The first assumption made is treating neutrino-nucleon scattering as an incoherent sum of scatterings from free nucleons. This approach is know as *impulse approximation* and any interference between the feynman diagrams of the individual neutrino-free nucleon scatterings are ignored.

Recalling the general form for the differential cross-section in equation 5.14

$$\frac{d\sigma}{dQ^2} = \frac{1}{64\pi E_\nu^2 M^2} \frac{G_F^2 \cos^2\theta_c}{4} \omega_{\mu\nu}\tau^{\mu\nu}$$

The effective hadronic tensor for the entire nucleus, $\omega_{\mu\nu}$, can be written as a sum of hadronic tensors describing the interactions of each of the nucleons with the neutrino, $\omega^i_{\mu\nu}$[62].

$$\omega_{\mu\nu} = \sum_i \int d^3p dE P(\boldsymbol{p}, E)\omega^i_{\mu\nu}(\tilde{p}, \tilde{q}) \tag{5.22}$$

The function $P(\boldsymbol{p}, E)$ is known as the target *spectral function* and it describes the probability distribution of having a nucleon with momentum $\boldsymbol{p}$ and requires energy, E, to be removed from the nucleus. The specific form the spectral function takes depends on the model of the nucleus and the nuclear model adopted here is the relativistic Fermi gas model.

5.4.1 Relativistic Fermi Gas (RFG) model

The nucleus is modelled as an ideal gas composed of weakly interaction fermions. The nucleons(neutrons and protons) are distinguishable fermions and they create two decoupled potentials.

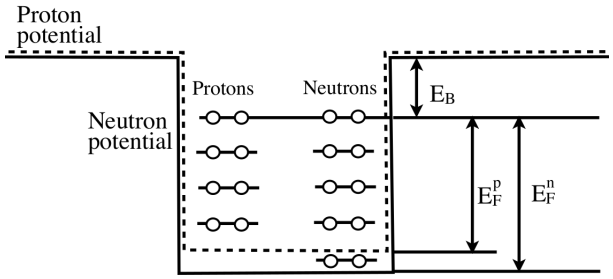

Figure 5.4: The proton and neutron potential wells and energy levels within the nucleus. The binding energy and Fermi momentum are adjusted with experimental data. Figure taken from [5]

In this simple model, the nucleon potentials are step-functions. The proton potential well is shallower than the neutron potential well as the protons experience Coulomb repulsion and require less energy to be ejected from the nucleus. Nevertheless, the protons and neutrons share the same Fermi surface, otherwise the nucleus will be unstable and undergo a series of β-decay until the Fermi energies of the protons and neutrons match up.

The spectral function for the RFG model is then[5]

$$P_{RFG}(\boldsymbol{p}, E) = \theta(p_F - |\boldsymbol{p}|)\delta(E_{|\boldsymbol{p}|} - M + E + E_B) \tag{5.23}$$

where $E_{|\boldsymbol{p}|}$ is the energy of the nucleon with momentum $\boldsymbol{p}$. E_B is the average binding energy, p_F is the Fermi momentum, and $E = -(E_B + E_F)$ is the ground state of the nucleon. Note that the protons and neutrons have different ground states within the nucleus. $\theta(x)$ is the Heaviside step function and it describes a flat Fermi momentum distribution for the nucleons within the nucleus.

5.4.2 Pauli blocking

The only condition for the spectral function in equation 5.23 is that the nucleons are not allowed to have momentums greater than the Fermi momentum, p_F. However, electron-nucleus scattering experiments showed that there is strong correlation between nucleons in the same nucleus. This results in excitation of nucleons to states with large momentums[63]. This correlation between the nucleons can be taken into account by adding a Pauli blocking function[64].

$$P_{RFG}(\boldsymbol{p}, E) = \theta(p_F - |\boldsymbol{p} + \boldsymbol{q}|)\theta(p_F - |\boldsymbol{p}|)\delta(E_{|\boldsymbol{P}|} - M + E + E_B) \tag{5.24}$$

The Pauli blocking term, $\theta(p_F - |\boldsymbol{p} + \boldsymbol{q}|)$, is a function of the momentums of the final nucleon states. The neutrino-nucleus interaction can leave nucleons excited, but with insufficient energy to be ejected from the nucleus. The final state of the excited nucleon must be one that is not already occupied, otherwise the interaction is not allowed.

Chapter 6

Radiative corrections in QED

Radiative corrections are higher-order contributions to the tree-level process from diagrams that contain loops. Bremsstrahlung is another source of radiative corrections and they involve the emission of final-state photons in a process. The corrections of order α to the total cross-section arises from the interference terms of the loop and bremsstrahlung diagrams with the tree-level diagram[65].

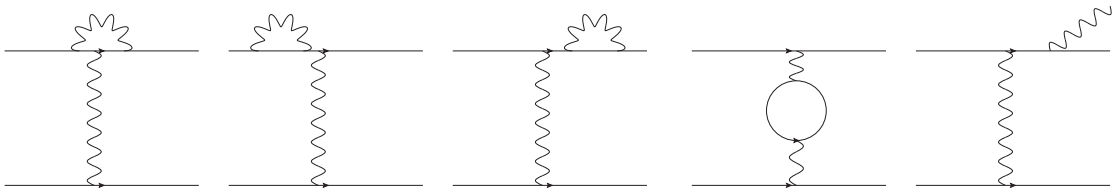

Figure 6.1: $\mathcal{O}(\alpha)$ corrections to tree-level cross-section come from interference of these diagrams with tree-level diagram.

The first diagram in figure 6.1 is known as the vertex correction and it gives rise to a plethora of effects such as the anomalous magnetic moment of the electron, which was first calculated by Schwinger in 1948. Measurements of the electron anomalous magnetic moment agree with the QED predictions up to more than 10 significant figures, making QED one of the most empirically tested theory in physics[66].

The second and third diagram in figure 6.1 give the first-order corrections to the external lepton legs. This eventually leads to a renormalisation of the lepton wavefunction and mass. The fourth diagram is associated to the self-energy of the photon and it leads to the renormalisation of the photon wavefunction and also a mass renormalisation if the regularization breaks gauge symmetry. Each of these 4 diagrams involves an integration over an undefined momentum loop. As the loop momentum increases ($k \to \infty$), particles of arbitrarily high momentum can appear in the loop, making the integral diverge in the ultraviolet region. Hence these diagrams are said to be UV divergent.

The last diagram is the bremsstrahlung diagram and it is divergent in the infrared region ($k \to 0$). This divergence is associated to the diverging probability of the lepton emitting a photon of arbitrarily low energy. It is crucial to include the bremsstrahlung diagrams when calculating physical cross-sections. The IR divergences of the bremsstrahlung diagrams will cancel the IR divergent pieces of the loop diagrams, giving an overall finite total cross-section, as illustrated in this section.

6.1 Bremsstrahlung

Bremsstrahlung refers to the radiation of photons from the charged final-state particles. The charged particles can emit an arbitrarily large number of photons. However, the cross-section of the process is suppressed by $\mathcal{O}(\alpha)$ for every additional photon radiated. Hence, it is reasonable to consider the first-order diagram where only one photon is emitted.

Let $\mathcal{M}_0$ denote the part of the amplitude that describes the coupling of the lepton legs to the hadronic legs.

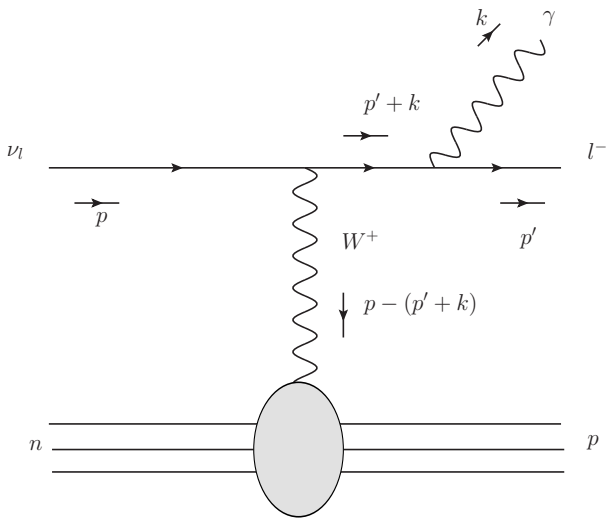

Figure 6.2: Low energy neutrinos interact with the bound nucleons and all the details of the interaction are represented by the grey blob, $\mathcal{M}_0$, which is a function of the momentum transfer.

The amplitude for the process described in figure 6.2 is then

$$i\mathcal{M} = -ie\bar{u}_{\text{charged lepton}}(p')\left[\gamma^\mu \epsilon^*_\mu(k)\frac{\not{p}' + \not{k} + m}{(p'+k)^2 - m^2}\mathcal{M}_0(p'+k,p)\right]u_{\text{neutrino}}(p) \qquad (6.1)$$

where m is the mass of the outgoing charged lepton and the momentums of the particles are as labelled in figure 6.2.

The scenario of interest involves the radiation of a soft photon that is beyond the sensitivity of the SK detector. The emission of a hard photon can be detected and those events are clearly distinct from the tree-level CCQE events. Hence the bremsstrahlung diagrams with hard photon emission will not contribute to the inclusive cross-section. It is then reasonable to assume that the photon radiated is soft $|\mathbf{k}| \ll |\mathbf{p'} - \mathbf{p}|$ and approximate

$$\mathcal{M}_0(p' + k, p) \approx \mathcal{M}_0(p', p) \tag{6.2}$$

The numerator of the propgator can be further simplified using the dirac equation and ignoring $\not{k}$.

$$\begin{aligned} \bar{u}_{\text{charged lepton}}(p')\gamma^\mu \epsilon^*_\mu (\not{p}' + m) &= \bar{u}(p')[2p'^\mu \epsilon^*_\mu + (-\not{p}' + m)\gamma^\mu \epsilon^*_\mu] \\ &= \bar{u}(p') 2p'^\mu \epsilon^*_\mu \end{aligned} \tag{6.3}$$

Summing over the two photon polarisation states,

$$d\sigma(p \to p' + \gamma) = d\sigma(p \to p') \int \frac{d^3k}{(2\pi)^3} \frac{1}{2k} \sum_{\lambda=1,2} e^2 \left| \frac{p'.\epsilon^{(\lambda)}}{p'.k} \right|^2 \tag{6.4}$$

The integral, which has an IR divergence, is regularised by introducing a small photon mass, μ and the following is obtained.

$$\frac{d\sigma}{d\Omega}(p \to p' + \gamma) = \left(\frac{d\sigma}{d\Omega} \right) \Big|_0 \left[1 + \frac{\alpha}{\pi} \log \left(\frac{-q^2}{m^2} \right) \log \left(\frac{-q^2}{\mu^2} \right) + \mathcal{O}(\alpha^2) \right] \tag{6.5}$$

The q^2 dependence of equation 6.5 is known as the *Sudakov double logarithm* and the dependence on the fictious photon mass, μ, poses a problem as one takes the limit of a physical massless photon, $\mu \to 0$. However, this problematic term will be cancelled by corrections from the vertex.

6.2 Electron vertex modification

There is only one type of vertex allowed in QED and this vertex receives corrections from both virtual lepton and photons.

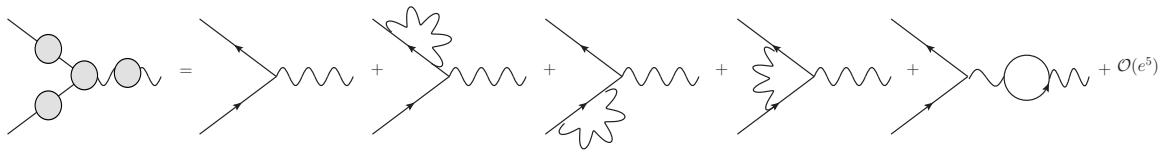

Figure 6.3: QED vertex up to one-loop corrections

The first diagram corresponds to the bare QED vertex. The second and third diagrams correspond to the self-energy corrections to the electron propagators, while the last diagram is associate with the self-energy correction to the photon propagator. The third diagram is referred to the vertex correction as such corrections cannot be wrapped up in any corrections to the propagators.

$$\bar{u}(p')\Gamma^{\mu}(p',p)u(p) = \bar{u}(p')\left[\gamma^{\mu}(p',p) + \delta\Gamma^{\mu}\right]u(p) \tag{6.6}$$

where

$$\begin{aligned}\Gamma^{\mu} &= \gamma^{\mu}A + (p'^{\mu} + p^{\mu})B + (p'^{m}u - p^{\mu})C \\ &= \gamma^{\mu}F_1(q^2) + \frac{i\sigma^{\mu\nu}q_{\nu}}{2m}F_2(q^2)\end{aligned} \tag{6.7}$$

A priori, the form of Γ^{μ} is restricted by Lorentz symmetry. The allowed form of Γ^{μ} is further simplified by using the Gordon identity of equation 5.13 and repackaged in terms of form factors, F_1 and F_2. The form factors are functions of the momentum transfer,$Q^2 = -q^2$, and they contain all the information about the charged lepton's effective electric charge and magnetic couplings. Form factors describe the dependence of interactions on the momentum transfer, without going into the full details of the underlying physics. This is particularly useful when there is a lack of theoretical models or when theoretical calculations become too cumbersome since form factors can be measured experimentally.

Concentrating on the leading order vertex correction,

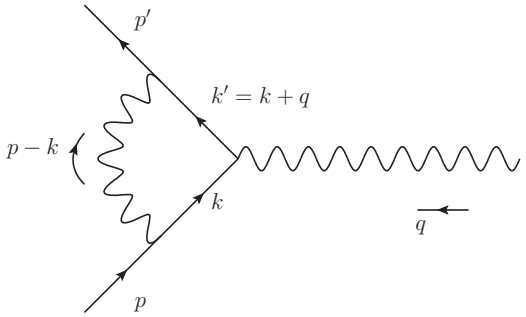

Figure 6.4: First order vertex correction

Naively applying the QED Feynman rules,

$$\begin{aligned}
&\bar{u}(p')\delta\Gamma^{\mu}(p',p)u(p) \\
&= \int \frac{d^4k}{(2\pi)^4}\frac{-ig_{\nu\rho}}{(k-p)^2+i\epsilon}\bar{u}(p')(-ie\gamma^{\nu})\frac{i(\not{k}'+m)}{k'^2-m^2+i\epsilon}\gamma^{\mu}\frac{i(\not{k}+m)}{k^2-m^2+i\epsilon}(-ie\gamma^{\rho})u(p) \\
&= 2ie^2\int \frac{d^4k}{(2\pi)^4}\frac{\bar{u}(p')[\not{k}\gamma^{\mu}\not{k}'+m^2\gamma^{\mu}-2m(k+k')^{\mu}]u(p)}{((k-p)^2+i\epsilon)(k'^2-m^2+i\epsilon)(k^2-m^2+i\epsilon)}
\end{aligned} \tag{6.8}$$

The evaluation of this integral is non-trivial, but it is made possible with the usage of Feynman parameter (see appendix equation A.3). The general strategy is to combine the denominator of equation 6.8 into a third power of a single polynomial in k. This allows one to perform a Wick rotation of the integral to turn it from Minkowskian to Euclidean, and subsequently evaluate it in spherical polars.
Introducing a Feynman parameter for each of the photon propagator terms, the denominator of equation 6.8 becomes

$$\begin{aligned}
\frac{1}{((k-p)^2+i\epsilon)(k'^2-m^2+i\epsilon)(k^2-m^2+i\epsilon)} &= \int_0^1 dxdydz\delta(x+y+z-1)\frac{2}{(l^2-\Delta+i\epsilon)^3} \\
&= \int_0^1 dxdydz\delta(x+y+z-1)\frac{2}{D^3}
\end{aligned} \tag{6.9}$$

where

$$l = k+yq-zp, \qquad D = l^2-\Delta+i\epsilon, \qquad \Delta = -xyq^2+(1-z)^2m^2 \tag{6.10}$$

The form of the numerator of equation 6.8 is restricted by Lorentz symmetry. Odd powers of l must vanish otherwise they will pick out some particular direction in space-time and break Lorentz invariance. Odd powers of q also vanish by the Ward-Takahashi identity. The numerator is then further simplified using the Dirac equation and the Gordon identity and becomes

$$\begin{aligned}
&\not{k}\gamma^{\mu}\not{k}'+m^2\gamma^{\mu}-2m(k+k')^{\mu} \\
&= \gamma^{\mu}(-\frac{1}{2}l^2+(1-x)(1-y)q^2+(1-4z+z^2)m^2)+\frac{i\sigma^{\mu\nu}q_{\nu}}{2m}(2m^2z(1-z))
\end{aligned} \tag{6.11}$$

Putting things together, equation 6.8 becomes

$$\begin{aligned}
&\bar{u}(p')\delta\Gamma^{\mu}(p',p)u(p) \\
&= 2ie^2\int\frac{d^4l}{(2\pi)^4}\int_0^1 dxdydz\ \delta(x+y+z-1)\frac{2}{D^3}\bar{u}(p') \\
&\quad\times\left[\gamma^{\mu}(-\frac{1}{2}l^2+(1-x)(1-y)q^2+(1-4z+z^2)m^2)+\frac{i\sigma^{\mu\nu}q_{\nu}}{2m}(2m^2z(1-z))\right]u(p)
\end{aligned} \tag{6.12}$$

However, when trying to evaluate the above integral in spherical polars after performing the Wick rotation (formula A.13), one then finds that the integral is divergent in the ultraviolet and infrared. This can be cured by regularising the integrals using the Pauli-Villars prescription, which essentially introduces fictious mass terms in the photon propagator. The rationale for choosing this regularization scheme is elaborated in A.9.
After all those mathematical gymnastics, a finite cross-section is finally obtained.

$$\frac{d\sigma}{d\Omega}(p \to p') = \left(\frac{d\sigma}{d\Omega}\right)\Big|_0 \left[1 - \frac{\alpha}{\pi}\log\left(\frac{-q^2}{m^2}\right)\log\left(\frac{-q^2}{\mu^2}\right) + \mathcal{O}(\alpha^2)\right] \tag{6.13}$$

Notice that this term is also divergent as $\mu \to 0$, but it cancels the divergence in equation 6.5 exactly. The IR divergence from the emission of arbitrarily soft real photons is cancelled by the vertex corrections arising from virtual photons and lepton loops. This is the Block-Nordsieck theorem, which states that the sum of the contributions from the virtual particles and soft photons will give a finite contribution[67]. At first sight, it may seem unsettling that diagrams with different number of vertices are added to cancel the IR divergence and that things may still blow up at higher orders. However, the IR divergence does cancel to all orders[68].

6.3 Radiative corrections to neutrino scattering

As the measured inclusive neutrino scattering cross-section becomes increasingly precise, the effects of electromagnetic radiative corrections starts to become significant. Inclusive cross-section refers to the sum of diagrams with the same ingoing particles/initial states but with different outgoing particles/final states. The inclusive cross-section is meaningful as some of the quantities (such as the energy and momentum of some of the final state particles) are not measured in an experiment. Also, physical detectors have finite energy resolution and they are unable to detect photons below a certain energy threshold. Hence, it will be useful to package these soft photons as part of the tree-level diagram via the inclusive cross-section.

The first calculations on the radiative corrections to charged-current neutrino scattering were done by Kiskis in 1973, which utilised a particular quark-proton model[6]. The corrections obtained had poorly defined terms like $\ln \frac{Q}{m_q}$ where Q is the momentum transfer and m_q is the quark mass. The definition of the quark mass is ambiguous. In particular, for $Q = 10GeV$, setting $m_q = 350MeV$ where the quark mass is interpreted as the constituent quark mass, yields a correction that is very different when setting $m_q = 1MeV$, which is the current algebra mass.

There were subsequent efforts in the community to investigate the dependence of such radiative corrections on the relatively unknown paramaters such as the quark mass. Notably in 1979, De Rujula claimed that most of the radiative corrections and physically

relevant questions are actually independent of the quark mass, and even the quark-model. This was achieved by using the leading log approximation along with other simplifying assumptions[69].

6.4 Contributing diagrams

Considering only the leading order diagrams, the diagrams that contribute to the radiative corrections to neutrino charged-current quasi-elastic scattering are as follow,

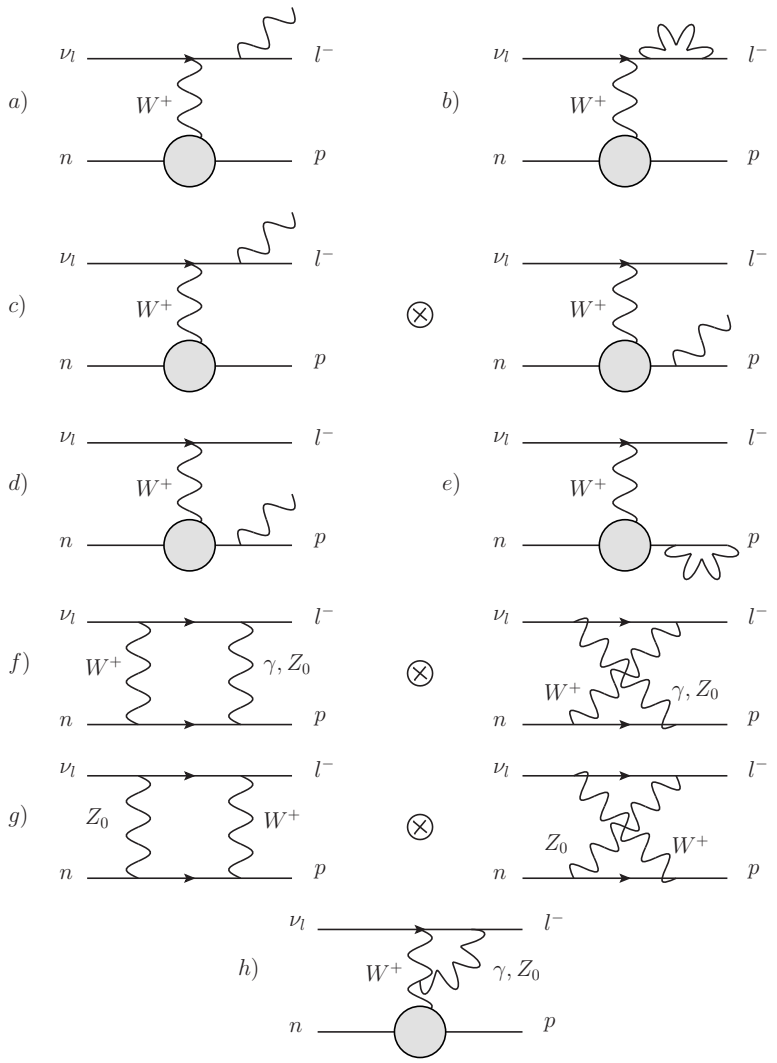

Figure 6.5: a: lepton leg bremsstrahlung, b: lepton propagator self-energy, c: interference, d: hadron leg bremsstrahlung, e: hadron propagator self-energy, f,g: two-boson exchange, h: gauge boson self-interactions.

The diagrams in figure 6.5 are not complete as the corrections to the weak intermediate vector bosons are not included. However, those diagrams will contribute terms of order $\mathcal{O}(\alpha Q^2/M_W^2)$ where M_W is the mass of the W boson. Hence these diagrams only contribute to higher order and can be neglected.

6.5 Leading log approximation

The radiative corrections become independent of the quark model and definition of quark mass in the leading log approximation. The relation between the observed cross-section, σ_{obs}, and the bare cross-section, σ_B, takes the following form,

$$\sigma_{obs} = \sigma_B + \underbrace{\frac{\alpha}{2\pi}\ln\frac{Q^2}{\mu^2}F\{\sigma_B\}}_{\text{lepton log}} + \underbrace{\frac{\alpha}{2\pi}\ln\frac{Q^2}{M^2}H}_{\text{hadron log}} + \underbrace{\frac{\alpha}{2\pi}G}_{\text{constant term}} \tag{6.14}$$

where μ is the charged-lepton mass, M is the nucleon mass, α is the electromagnetic coupling constant and Q is the energy scale of the overall process.

Conventionally, leading log refers to all terms up to order, $\mathcal{O}\left[\frac{\alpha}{\pi}\ln\frac{Q^2}{M^2}\right]^n$. However, in this leading log approximation, only contributions from the lepton log is considered. The lepton log arises from the emission of collinear soft photons. Looking at equation 6.4, the momentum of the undetected soft photons is integrated over, giving rise to the following factor

$$\int \frac{d^3k}{2k}\frac{1}{p'\cdot k} \sim \int_0^1 d\cos\theta \frac{1}{E_\mu k\left(1-\frac{|\boldsymbol{p}'_\mu|\cos\theta}{E_\mu}\right)} \tag{6.15}$$

The outgoing lepton is ultra-relativistic, $|\boldsymbol{p}'_\mu| \sim E_\mu$ and the expression diverges as $\cos\theta \to 1$. This corresponds to the emission of photons that are almost parallel to the charged lepton. The lepton log factorises and the leading corrections only depend on the momentum distribution of the outgoing charged lepton. The coefficient of the lepton log, $F\{\sigma_B\}$, is a functional of the bare cross-section and can be computed from data.

The hadron leg also factorises and its potentially large contribution only comes from the diagrams involving the hadron leg. Hadron leg corrections only arise when one tries to discern the hadrons from the real collinear or virtual photons in the hadron shower. The final-state hadrons are often not detected in neutrino oscillation experiments and hence it is justified to ignore the contribution from the hadron leg to the overall radiative corrections.

The constant term is dependent on the model used to describe the strong interactions within the nucleus, making it non-trivial to calculate. However, the constant term only scales the cross-section up and down and can be interpreted as an overall normalisation factor.

6.6 Double differential cross-section

Dividing the cross-section by the allowed phase space of the outgoing charged lepton, the double differential cross-section of the radiatively corrected process is[69]

$$\frac{d\sigma_{LLL}}{dE_l d\Omega} = \frac{d\sigma_B}{dE_l d\Omega} + \frac{\alpha_{EM}}{\pi} \ln \frac{2E_l^*}{m} \int_0^1 \frac{1+z^2}{1-z} \left(\frac{1}{z} \frac{d\sigma_B}{d\hat{E}_l d\Omega} \bigg|_{\hat{E}_l = E_l/z} - \frac{d\sigma_B}{dE_l d\Omega} \right) dz \qquad (6.16)$$

where z is the fraction of energy the charged lepton retains after emitting the soft collinear photon. E_l^* is the final-state energy of the charged lepton in the center-of-mass frame.

The leading log corrections arise from collinear emission of photons in the lepton legs. The emission of photons moves events from a large to a smaller outgoing lepton energy, E_μ while keeping the angle between the outgoing lepton and the incoming neutrino fixed since the emitted photons are collinear with the outgoing charged lepton.

In a physical gauge, the first term in the integrand corresponds to the contribution from bremsstrahlung diagrams(see diagram (a) in figure 6.5). The second term in the integrand comes from the charged lepton self-energy diagrams(see diagram (b) in figure 6.5). The bremsstrahlung term is divergent as $z \to 0$ and this is the IR divergence discussed in section 6.1. However, in the soft photon limit, the infrared singularity is cancelled by the self-energy term. Summing the contributions from both real and virtual photons, a finite correction is obtained. This is an important result which will be explored further via simulations described in the following chapter.

Chapter 7

Simulations

Using realistic input muon neutrino flux predictions, muon neutrino interactions were generated using a neutrino interactions generator, NEUT. The double differential cross-sections for the charged-current quasi-elastic (CCQE) interactions were then extracted and the radiative corrections to the CCQE events were calculated using the result equation 6.16 discussed in the previous chapter. The graphs obtained were created using ROOT, a data analysis and graphics package written in C++ that is widely used in High Energy Physics.

7.1 Software

7.1.1 NEUT

Written mainly in FORTRAN77, NEUT is a neutrino interaction simulation library which was first developed to study atmospheric neutrino and nucleon decay in Kamiokande. It was subsequently updated for the Super-Kamiokande and K2K experiment, both of which used water-based Cherenkov detectors to detect neutrino interactions. Even though NEUT was designed with neutrino interactions with protons and oxygen nuclei in mind, it is capable of generating neutrino interactions with other nuclei as well[70].

The list of neutrino interactions that can be selected in NEUT is as follows:

CC/NC (quasi-)elastic scattering $\quad \nu + N \rightarrow l + N'$
CC/NC single meson(π, K, η) production $\quad \nu + N \rightarrow l + N' + \text{meson}$
CC/NC deep inelastic scattering $\quad \nu + N \rightarrow l + N' + \text{hadrons}$
CC/NC coherent pion production $\quad \nu + {}^{16}O \rightarrow l + {}^{16}O + \pi$
where CC and NC refer to charged current and neutral current respectively. N and N' are the interaction target nucleons and l is the charged lepton.

The calculation of interest is the radiative corrections to charged-current quasi-elastic(CCQE) interactions and hence only the first mode was explored. The CCQE interactions were simulated based on the Llewellyn-Smith formalism, which was described in section 5.3.1. The vector and axial-vector form factors are assumed to take the dipole form. The SK detetor is filled with pure water and hence the neutrinos interact mainly with ^{16}O nuclei. The nuclear effects of the ^{16}O nuclei were taken into account using the relativistic Fermi Gas model and Pauli blocking described in sections 5.4.1 and 5.4.2 respectively.

7.2 Code structure and Findings

The radiative corrections to the CCQE interactions are calculated using equation 6.16, where the radiative correction term is

$$\frac{d\sigma_{LLL}}{dE_l d\Omega} - \frac{d\sigma_B}{dE_l d\Omega} = \frac{\alpha_{EM}}{\pi} \ln \frac{2E_l^*}{m} \int_0^1 \frac{1+z^2}{1-z} \left(\frac{1}{z} \frac{d\sigma_B}{d\hat{E}_l d\Omega} \bigg|_{\hat{E}_l = E_l/z} - \frac{d\sigma_B}{dE_l d\Omega} \right) dz \tag{7.1}$$

The crux of this calculation lies in the calculation of the double differential cross-section, $\frac{d\sigma}{dEd\Omega}$.

7.2.1 Double differential cross-section

While it is not impossible to analytically calculate the double differential cross-section of the CCQE scattering while incorporating the nuclear effects from the target nuclei, a more tractable task is to extract the double differential from the Monte Carlo(MC) events generated by NEUT.

To generate events, NEUT requires several input parameters which are defined in a card file. The important input parameters are summarised in the following table.

Input parameter	**Value**
No. of events	10 million
Neutrino type	Muon neutrino
Neutrino momentum	Randomly sampled from SK muon neutrino flux prediction (figure 7.1)
Target nuclei	Water (8 bound protons, 8 bound neutrons, 2 free protons)
Neutrino modes	All modes turned on
Fermi motion	Turned on
Pauli blocking	Turned on
CCQE vector mass	0.84 GeV
CCQE axial mass	1.21 GeV

Table 7.1: Important input parameters for NEUT. The input card codes found in Appendix B shows the full list of input parameters and options available in NEUT. The full analysis code and shell scripts are available upon request.

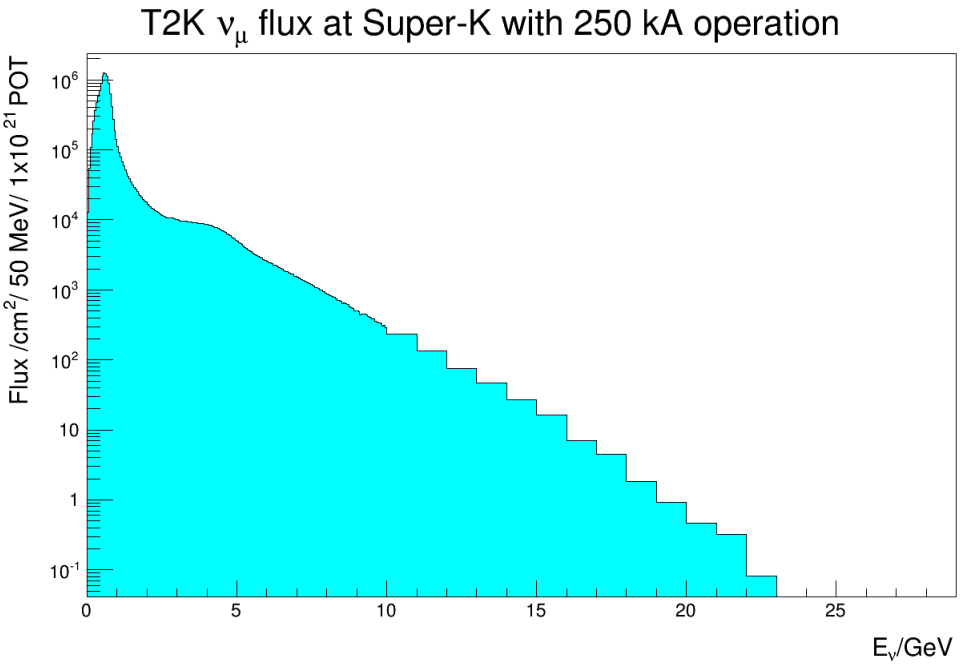

Figure 7.1: Muon neutrino flux prediction at the SK detector. Data taken from [4]. The flux can be split into three regions. Most of the muon neutrinos have energies below 2 GeV, a substantial amount of them have energies from 2 GeV to 10 GeV and a trace amount have energies above 10 GeV but below 23 GeV. The flux is peaked at 0.6 GeV.

The double differential cross-section is extracted from a sample of 10 million MC events in which all possible neutrino interaction modes are turned on. It is important to include all the interaction modes so as to not artificially inflate the CCQE cross-section. The generated MC events are stored in a `.root` file and analysed using ROOT. The number of CCQE events per outgoing muon kinetic energy per solid angle is stored in an one-dimensional histogram. This histogram is then normalised using the flux according to the following expressing to yield the double differential cross-section.

$$\frac{18}{8}\frac{\sum_i N_i}{\sum_i \Phi_i}\frac{\text{No. events in bin}}{\text{Total no. events}}\frac{1}{\text{bin area}} \tag{7.2}$$

where the summation is over all the neutrino energy bins in the histogram. N_i is the event rate in the i-th energy bin, which is defined as the cross-section multiplied by the flux, Φ_i, at that particular neutrino energy. The cross-section in NEUT is defined per neutron and given in units of 10^{-38}cm^2. The numerical prefactor takes into account that there are 18 nucleons with 8 neutrons in the target water nucleus. The last factor divides the cross-section by the bin area to turn it into a double differential cross-section. An example of the extracted double differential cross-section is shown in figure 7.2.

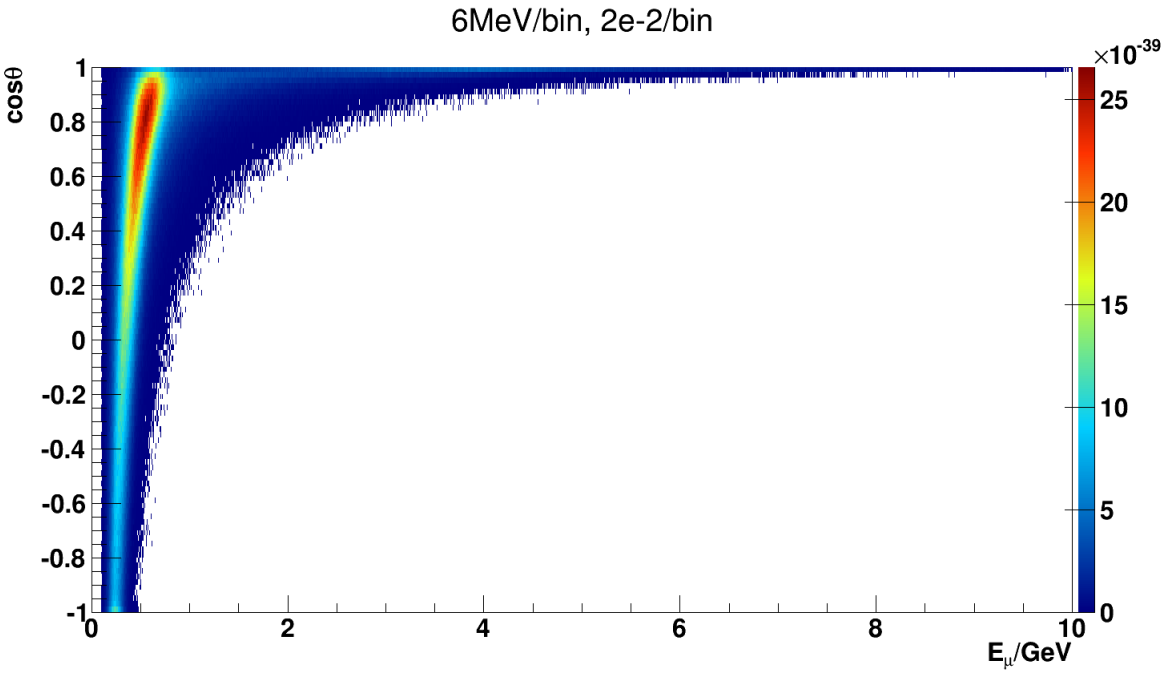

Figure 7.2: θ is the deflection angle between the incoming neutrino and outgoing muon, while E_μ is the outging muon energy. The z-axis gives the cross-section(cm^2) for muon neutrino CCQE scattering in each bin in the event kinematics space.

7.2.2 Optimisation

Calculation of radiative corrections highly sensitive to accuracy of the extracted double differential cross-section. The accuracy of the double differential cross-section is dependent on the way it is stored. The double differential cross-section is stored in a 2D histogram and the free parameters are the bin sizes of the histogram along the two axes. Another free parameter is the step size when integrating over z when calculating the radiative correction. These free parameters are optimised to minimise the fraction of problematic events.

There are two identified classes of problematic events.

Type I: Sparse events

Looking at the right-hand side of equation 7.1, the calculation of the radiative corrections requires taking the difference of the cross-sections evaluated at the energy of the muon before, $\hat{E}_l$, and after emitting the photon, E_l. The first type of problematic events are events in which either of the double differential cross-sections, $\frac{d\sigma_B}{d\hat{E}_l d\Omega}$ or $\frac{d\sigma_B}{dE_l d\Omega}$, is zero. Such events are common near the fuzzy edges of the double differential cross-section histogram, where the histogram is sparsely populated.

One way to minimise Type I problematic events is to increase the bin size of double differential cross-section histogram. However, this compromises on the accuracy of the calculation. More detrimentally, there is a limit to which the bin sizes can be increased before E_l and $\hat{E}_l$ end up in the same energy bin, returning a trivial radiative correction when the correction is actually non-zero.

Type II: High Q^2 events

The second type of problematic events are associated with events at constant high momentum transfer, Q^2. The double differential cross-section is non-zero and distinct at both E_l and $\hat{E}_l$ for these events and further investigations are required to probe why the calculation fails for such events.

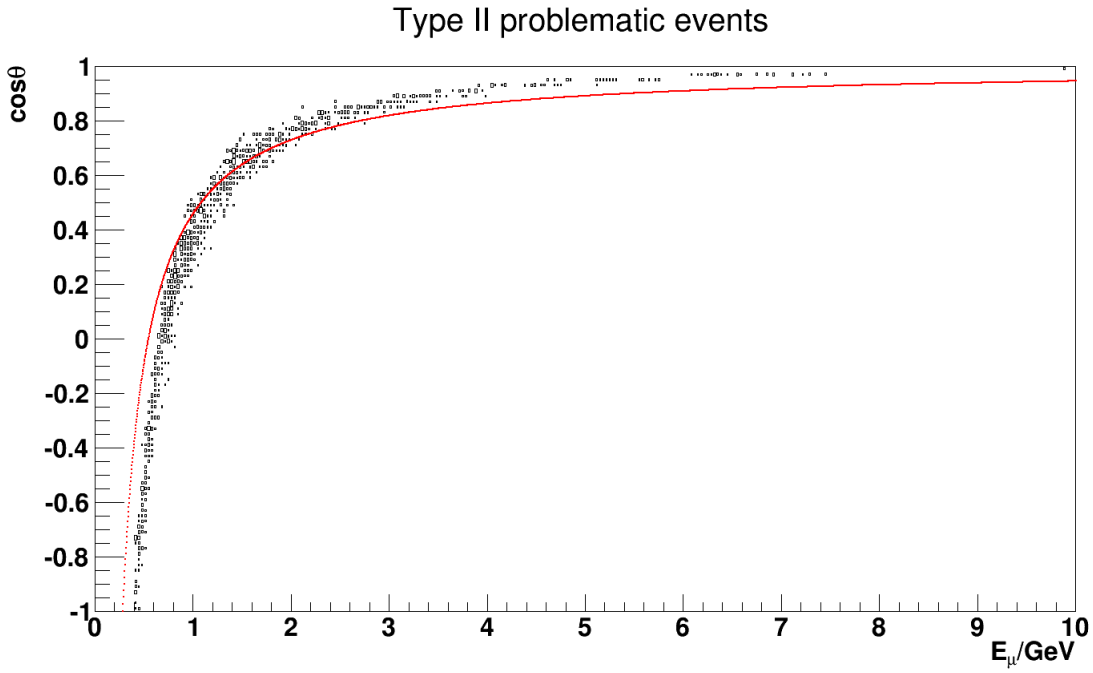

Figure 7.3: Problematic events at high Q^2. The boxes reflect the distribution of type II problematic events. The line overlaid is a curve constant neutrino energy, $E_\nu = 0.6$ GeV, and constant momentum transfer, $\sqrt{Q^2} = 0.8$ GeV. Most of the CCQE events have momentum transfer $\sim \sqrt{Q^2} = 0.4$ GeV.

A series of bin sizes were explored before deciding on the binning scheme of (6MeV/bin, 2e-2/bin). The number of problematic events for the various binning schemes can be found in table C.1 in appendix C.

z steps

Looking again at equation 7.1, the difference between the double differential cross-section at E_l and $\hat{E}_l$ is then integrated over all possible energy fraction retained by the muon, z, while weighted by the QED splitting function, $\frac{1+z^2}{1-z}$. This integral is carried out numerically by doing a Riemannian sum and the integration step size, Δz, is a free parameter in this calculation. A range of values for Δz is tested and it is found that increasing the number of integration steps does not decrease the number of problematic events drastically. The results of this parameter search can be found in table C.2. Subsequent analysis are carried out with the coarsest integration step-size, $\Delta z = 0.02$, to reduce the time required to complete the computation.

7.2.3 Radiative correction calculations

After optimising the extraction of the double differential cross-section, the the radiative correction calculation is carried out on a sample of 1 million MC events. This sample is generated with only the pure CCQE mode turned on but keeping other input parameters the same as summarised in table 7.1. The other neutrino interaction modes are only relevant for obtaining the correct normalisation during the extraction of the double differential cross-section. For each event in the sample, the radiative correction is calculated by direct application of equation 7.1.

The absolute value of the double differential cross-section is very small and on the order of $\mathcal{O}(10^{-40})$ cm^2. A more meaningful quantity to examine is the fractional radiative corrections, δ_{radcor}, which is defined as

$$\delta_{radcor} \equiv \frac{\frac{d\sigma_{LLL}}{dE_l d\Omega} - \frac{d\sigma_B}{dE_l d\Omega}}{\frac{d\sigma_B}{dE_l d\Omega}} \tag{7.3}$$

The definition of the fractional radiative corrections makes it easy to apply to analysis as the corrected double differential cross-section is related to the uncorrected double differential cross-section via a simple multiplicative factor.

$$\frac{d\sigma_{LLL}}{dE_l d\Omega} = (1 + \delta_{radcor}) \frac{d\sigma_B}{dE_l d\Omega} \tag{7.4}$$

The fractional radiative corrections is calculated for each event in the sample of pure CCQE events and stored in a 2D histogram. The binning scheme of this histogram does not affect the value of the calculated radiative corrections drastically since the value in each bin is an averaged value of the radiative correction to all the events that fall within that bin. Figure 7.4 shows the averaged radiative corrections calculated on a sample of 1 million CCQE events, with the all Type I problematic events skipped and Type II probematic events skipped if the resulting fractional radiative corrections is greater than unity.

Looking at figure 7.1, the bulk of the muon neutrinos arriving at the SK detector have energies less than 2 GeV. Therefore, a significant amount of the muons produced in the neutrino-target nuclei interactions have energies less than 2 GeV. Focusing on events with muon energies in the range of interest, the fractional radiative corrections is presented in figure 7.4.

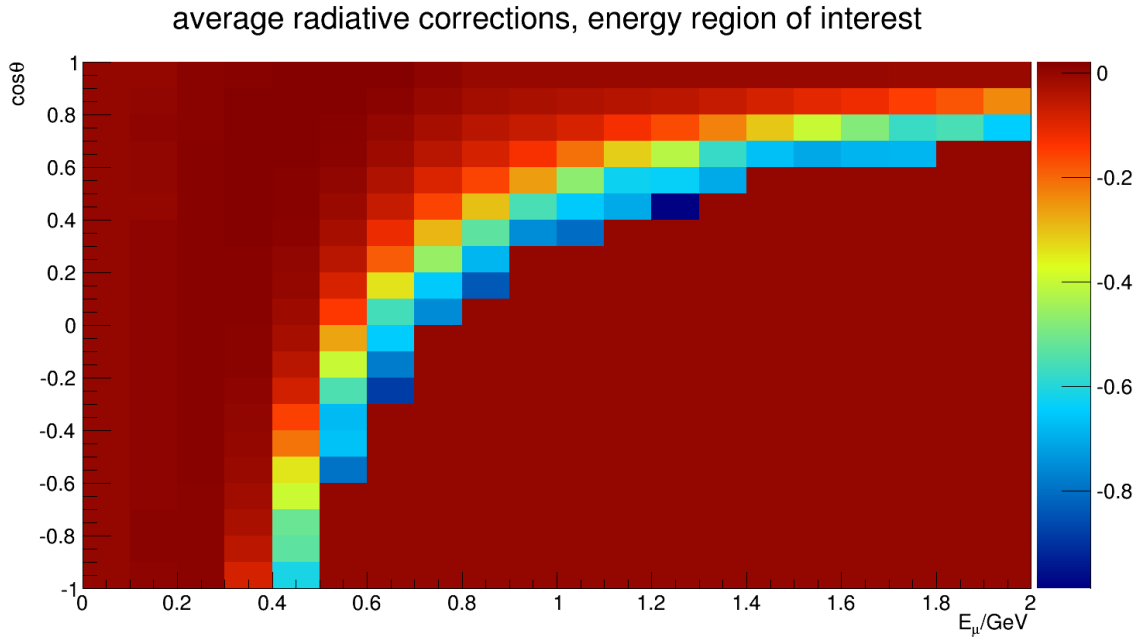

Figure 7.4: The fractional radiative corrections as defined in equation 7.3 is represented by the z-axis. The value of the radiative corrections in each bin can be found in table C.3 in Appendix C.

Figure 7.4 suggests that low energy muons($E_\mu < 0.3$ GeV) receive small positive radiative corrections while energetic forward moving muons receive large positive corrections.

The radiative corrections obtained are dependent on both the energy and direction of the outgoing muon. The energetic muons, $E_\mu > 0.4$ GeV receive a negative radiative corrections while the muons with energies, E_μ <0.4 GeV, receive small positive corrections on the order of $\sim 1\%$. A possible explanation to this is that energetic muons are more likely to radiate off photons and the double differential cross-section is greater after the emission of photons than before emitting the photons. Conversely, at low muon energies, $E_\mu < 0.4$ GeV, the muons are less likely to radiate off photons. This is avoids the IR singularity as it the probability of the muon radiating off a photon vanishes as the photon becomes arbitrarily soft. This trend of changing signs for the radiative corrections is also reported in a very recent study on radiative corrections to CCQE[2].

In the the peak muon energy bin($0.5 < E_\mu$0.6 GeV), the radiative correction is -22.41%, which is non-trivial. There is a known small difference between total CCQE cross-section measurements and NEUT predictions of $\sim -7.14\%$. This value is obtained from the numbers read off figure 13 in [71]. Further investigations are needed to convert the

radiative corrections on the double differential cross-section to corrections on the total cross-section before a justified comparison can be made between the value obtained in this study and the discrepancy observed in [71].

The radiative corrections are dependent on the direction of the outgoing muons. The forward going muons, $0.9 < \cos\theta < 1.0$, receive small corrections regardless of their energie. For $0.9 < \cos\theta < 1.0$, the corrections are 0.14% for muons with $0.1 < E_\mu < 0.2$ GeV and -0.84% for energetic forward muons with $1.9 < E_\mu < 2.0$ GeV. Energetic muons that undergo large deflections, $-0.3 < \cos\theta < -0.2$ and $0.6 < E_\mu < 0.7$, receive large corrections of -88.50%. This is reminiscent of classical bremsstrahlung in which charged particles that are more accelerated radiate more.

7.3 Conclusions

The radiative corrections obtained for muon neutrino CCQE interactions are found to be dependent on both the energy and direction of the outgoing muon. The muons that are greatly deflected receive greater radiative corrections and is suggestive of classical bremsstrahlung. The radiative corrections at the peak muon energy at the SK detector is found to be -22.41% which is not small but further detailed investigations are required before comparing it to the observed discrepancy between data and simulations. It is also interesting to note the change in sign of the radiative corrections with increasing muon energy and how this is possibly the manifestation of the cancellations between diagrams containing virtual photons and soft photons that makes the theory IR safe.

7.4 Recommendations

Recall from chapter 4 that precise measurements of the neutrino mixing angle, θ_{13} and the CP-violating phase, δ, are made from observing $\nu_\mu \to \nu_e$ oscillations. Neutrinos are detected primarily through their CCQE interactions with the target nuclei in the detector, hence, it is important to understand the difference between muon neutrino interactions and electron neutrino interactions well so that the two different neutrino flavours are well distinguished.

It will be interesting to extend this study to incoming electron neutrinos and investigate if radiative corrections can alter the difference between the cross-section of an electron neutrino interaction and a muon neutrino interaction. Note, however, that electrons are ~ 200 times lighter than muons and the energy lost during the electrons' propagation can be as large as the radiative corrections[69]. Also, if such QED radiative corrections are significant, the calculation can also be extended to include the two-boson exchange diagrams shown in figure 6.5.

Appendix A

Useful mathematical tools

A.1 Gamma matrix properties

The gamma matrices are defined by the Clifford algebra

$$\{\gamma^\mu, \gamma^\nu\} = \gamma^\mu\gamma^\nu + \gamma^\nu\gamma^\mu = 2\eta^{\mu\nu}\mathbb{1}_4 \tag{A.1}$$

The following useful properties of the gamma matrices will be utilised when calculating cross-sections for scattering processes.

$Tr(\text{odd no. of } \gamma_\mu) = 0$
$Tr(\gamma_5 \text{ odd no. of } \gamma_\mu) = 0$
$Tr(\not{a}\not{b}\not{c}\not{d}) = 4[(a\cdot b)(c\cdot d) - (a\cdot c)(b\cdot d) + (a\cdot d)(b\cdot c)]$
$Tr(\gamma_5) = 0$
$Tr(\gamma_5\not{a}\not{b}) = 0$
$Tr(\gamma_5\not{a}\not{b}\not{c}\not{d}) = 4i\epsilon_{\mu\nu\lambda\sigma}a^\mu b^\nu c^\lambda d^\sigma$
$\gamma_\mu\not{a}\gamma^\mu = -2\not{a}$
$\gamma_\mu\not{a}\not{b}\gamma^\mu = 4a\cdot b$
$\gamma_\mu\not{a}\not{b}\not{c}\gamma^\mu = -2\not{c}\not{b}\not{a}$
$Tr(\gamma^\mu\not{p}_1\gamma^\nu\not{p}_2) = 4[p_1^\mu p_2^\nu + p_1^\nu p_2^\mu - (p_1\cdot p_2)g^{\mu\nu}]$
$Tr(\gamma^\mu(1-\gamma_5)\not{p}_1\gamma^\nu(1-\gamma_5)\not{p}_2) = 2Tr(\gamma^\mu\not{p}_1\gamma^\nu\not{p}_2) - 8i\epsilon^{\mu\nu\lambda\sigma}p_{1\lambda}p_{2\sigma}$
$Tr(\gamma^\mu\not{p}_1\gamma^\nu\not{p}_2)Tr(\gamma_\mu\not{p}_3\gamma_\nu\not{p}_4) = 32[(p_1\cdot p_3)(p_2\cdot p_4) + (p_1\cdot p_4)(p_2\cdot p_3)]$
$Tr(\gamma^\mu\not{p}_1\gamma^\nu\gamma_5\not{p}_2)Tr(\gamma_\mu\not{p}_3\gamma_\nu\gamma_5\not{p}_4) = 32[(p_1\cdot p_3)(p_2\cdot p_4) - (p_1\cdot p_4)(p_2\cdot p_3)]$
$Tr(\gamma^\mu(1-\gamma_5)\not{p}_1\gamma^\nu(1-\gamma_5)\not{p}_2)Tr(\gamma_\mu(1-\gamma_5)\not{p}_3\gamma_\nu(1-\gamma_5)\not{p}_4) = 256(p_1\cdot p_3)(p_2\cdot p_4)$

A.2 $SU(2) \times U(1)$ generators

$$\tau_1 = \begin{pmatrix} 0 & 1 \\ 1 & 0 \end{pmatrix} \qquad \tau_2 = \begin{pmatrix} 0 & -i \\ i & 0 \end{pmatrix} \tag{A.2}$$

$$K \equiv \frac{\tau_3 - y}{2} = \begin{pmatrix} 0 & 0 \\ 0 & -1 \end{pmatrix} \qquad Q \equiv \frac{\tau_3 + y}{2} = \begin{pmatrix} 1 & 0 \\ 0 & 0 \end{pmatrix} \tag{A.3}$$

A.3 Feynman Parameters

$$\frac{1}{AB} = \int_0^1 \frac{1}{xA + (1-x)B^2} = \int_0^1 dxdy\delta(x+y-1)\frac{1}{[xA+yB]^2} \tag{A.4}$$

Differentiating A.4 with respect to B,

$$\frac{1}{AB^n} = \int_0^1 dxdy\delta(x+y-1)\frac{ny^{n-1}}{[xA+yB]^{n+1}} \tag{A.5}$$

Repeated differentiation of A.5 will give

$$\frac{1}{A_1...A_n} = \int_0^1 dx_1...dx_n\ \delta\left(\Sigma x_i - 1\right)\frac{(n-1)!}{[x_1A_1 + ... + x_nA_n]^n} \tag{A.6}$$

The most general identity is

$$\frac{1}{A_1^{m_1}...A_n^{m_n}} = \int_0^1 dx_1...dx_n\ \delta\left(\Sigma x_i - 1\right)\frac{\Pi x_i^{m_i-1}}{[\sum x_iA_i]^{\Sigma m_i}}\frac{\Gamma(m_1 + ... + m_n)}{\Gamma(m_1)...\Gamma(m_n)} \tag{A.7}$$

where the m_i do not have to be integers. The identity given in A.7 is overkill and is given only for completeness. It is not used anywhere in this paper.

A.4 Regularisation schemes

Quantum Field Theory is plagued by divergences, but those badly behaved integrals can be regulated and made finite in a number of ways.
The most intuitive way to regularise a diverging integral is to impose a cut-off and limit the integration over the loop momentum up to $k^2 \leq \Lambda^2$ instead of infinity. However, this way of regularisation is very intrusive as it breaks many symmetries such as translational invariance in the momentum space $p \to p + k$. This is not desirable as translational invariance in momentum space is required for combining many propagators into a single one using Feynman parameters. The momentum cutoff also breaks gauge invariance, which makes calculations cumbersome as one cannot then use the Ward-Takahashi identity to kill off stray terms.
Pauli-Villars regularisation is another way of regularising a diverging integral. It involves subtracting from the photon propagator, the propagator of a particle with a much larger mass. This substraction can be interpreted as the propagator correction from a ghost field with the same quantum numbers as the original field but with opposite statistics. The ghost field then decouples from the theory at energies very much lower than its mass, M. This regularisation method has the advantage of keeping translational invariance in the momentum space. However, the Pauli-Villars prescription is not gauge covariant due to the very nature of introducing a mass term.

$$\frac{1}{(k-p)^2 + i\epsilon} \longrightarrow \frac{1}{(k-p)^2 + i\epsilon} - \frac{1}{(k-p)^2 - \Lambda^2 + i\epsilon} \tag{A.8}$$

There is also dimensional regularisation, in which badly behaved integrals are evaluated over d-dimensional spacetime, instead of the usual 4 dimensions. The physical theory is then recovered by setting $d = 4 - \epsilon$ and taking limits of $\epsilon \to 0$. This method of regularisation is more common in modern literature as it is more mathematically elegant and is compatible with more symmetries, making it computationally more efficient. Its main setback is that is it very involved and often physical intuition of the theory is lost when the number spacetime dimensions take on non-integer values.
Remaining in 4-dimensional spacetime, the IR divergence encountered when calculating the first order QED vertex correction by introducing a small mass, μ, to the photon propagator.

$$\frac{1}{(k-p)^2 + i\epsilon} \longrightarrow \frac{1}{(k-p)^2 - \mu^2 + i\epsilon} \tag{A.9}$$

A.5 Wick rotation

Wick rotation is a mathematical technique common used for evaluating integrals which are otherwise cumbersome to evaluate in Minkowskian spacetime due to its pseudo-Riemannian metric of signature (1,3). By making time imaginary, Wick rotation turns the integral over Minkowskian spacetime into an integral over Euclidean space. The Euclidean integral can then be integrated in 4-dimensional spherical polar coordinates.

$$k^0 = ik_E^0, \qquad \mathbf{k} = \mathbf{k_E} \tag{A.10}$$

For example in 4-dimensional space-time,

$$\int \frac{d^4k}{(2\pi)^4} \frac{1}{[k^2-\Delta]^m} = \frac{i(-1)^m}{(4\pi)^2} \int d\Omega_4 \int_0^\infty dk_E \frac{k_E^3}{[k_E^2+\Delta]^m} \tag{A.11}$$

The pole on the real axis at $k^2 = \Delta$ is avoided by making time imaginary and integrating along the imaginary axis instead. Explicit evaluation of this integral gives

$$\int \frac{d^4k}{(2\pi)^4} \frac{1}{[k^2-\Delta]^m} = \frac{i(-1)^m}{(4\pi)^2} \frac{1}{(m-1)(m-2)} \frac{1}{\Delta^{m-2}} \tag{A.12}$$

Another useful formula is

$$\int \frac{d^4k}{(2\pi)^4} \frac{k^2}{[k^2-\Delta]^m} = \frac{i(-1)^{m-1}}{(4\pi)^2} \frac{2}{(m-1)(m-2)(m-3)} \frac{1}{\Delta^{m-3}} \tag{A.13}$$

The case for $m = 3$ after regularization using the Pauli-Villars prescription

$$\int \frac{d^4k}{(2\pi)^4} \left[\frac{k^2}{[k^2-\Delta]^3} - \frac{k^2}{[k^2-\Delta_\Lambda]^3} \right] = \frac{i}{(4\pi)^2} \log\left(\frac{\Delta_\Lambda}{\Delta}\right) \tag{A.14}$$

Appendix B

NEUT card file

```
C====================================================================
C  Input card for Super-Kamiokande Monte Carlo simulation
C====================================================================
C
C Number of events ; EVCT-NEVT
C
EVCT-NEVT  1000000
C
C--------------------------------
C
C Particle Code ; EVCT-IDPT
C
EVCT-IDPT 14
C
C--------------------------------
C
C fixed  VERTEX ; EVCT-MPOS 1
C random VERTEX ; EVCT-MPOS 2
C
C EVCT-MPOS 1
C VECT-POS  100. 0. 0.
C
EVCT-MPOS 2
EVCT-RAD  100.
C
C--------------------------------
C
C fixed  DIRECTION ; EVCT-MDIR 1
C random DIRECTION ; EVCT-MDIR 2
C
EVCT-MDIR 1
EVCT-DIR 0. 0. 1.
C
C
C--------------------------------
C
C fixed  MOMENTUM ; EVCT-MPV 1
C random MOMENTUM ; EVCT-MPV 2
C
C random MOMENTUM based on flux times cross section distribution
C EVCT-MPV 3
C EVCT-FILENM : name of ROOT file containing flux histogram
```

```
C EVCT-HISTNM : flux histogram name
C EVCT-INMEV  : flag for histograms in MeV
C               (MeV => 1, GeV => 0)
C
CEVCT-MPV 1
CEVCT-PV  400.
CEVCT-MPV 2
CEVCT-PV  0. 200.
C
EVCT-MPV 3
EVCT-FILENM  't2kflux_2013_horn250kA.root'
EVCT-HISTNM  'enu_sk_numu'
EVCT-INMEV 0
C
C
C **** TARGET INFORMATION ****
C
C NUMBNDN : total number of neutron
C           (e.g. CH => 6, H2O => 8, Ar => 22, Fe => 30)
C
NEUT-NUMBNDN 8
C
C NUMBNDP : total number of bound proton
C           (e.g. CH => 6, H2O => 8, Ar => 18, Fe => 26)
C
NEUT-NUMBNDP 8
C
C NUMFREP : total number of free proton
C           (e.g. CH => 1, H2O => 2, Ar => 0, Fe => 0)
C
NEUT-NUMFREP 2
C
C NUMATOM : atomic number of atom heavier than hydrogen
C           (e.g. CH => 12, H2O =>16, Ar => 40, Fe => 56)
C
NEUT-NUMATOM 16
C
CNEUT-PFSURF 0.217
CNEUT-PFMAX  0.217
CNEUT-VNUINI -.034
C
C **** NEUTRINO INTERACTION ****
C
C FERM : Fermi motion  0 : on ( default )  1 : off
C
NEUT-FERM 1
C
C PAUL : Pauli blocking  0 : on ( default )  1 : off
C
NEUT-PAUL 1
C
C NEFF : Nuclear effect in O16  0 : on ( default )  1 : off
C
NEUT-NEFF 0
C
C IFORMLEN : Formation zone 1: on (default) 0: off
C
NEUT-IFORMLEN 1
C
C Resonant Pion-less Delta Decay (20% Default)
C   IPILESSDCY: 1: on (default), 0: off
C   RPILESSDCY: Fraction of 1pi events (0.2 default)
C
NEUT-IPILESSDCY 1
```

```
NEUT-RPILESSDCY 0.2
C
C
C ABSPIEMIT : Nucleon emission after absorption of pi 1: on (default) 0: off
C
NEUT-ABSPIEMIT 1
C
C
C NUSIM : Toggle neutrino simulation or not (piscat/gampi) 1: yes (default) 0: no
C
NEUT-NUSIM 1
C
CCCCCCCCCCCCCCCCCCCCCCCCCCCCCCCCCCCCCCCCCCCCCCCCCCCCCCCCCCCCCCCCCCCCCCCCCCCCCCCC
C
C MODL : Toggle between low energy pion mean free path models
C ( momentum of pi < 500MeV/c, but also add absorption for p > 500 MeV/c)
C                 0: Salcedo et al. calculation (used in productions prior to 2011)
C                 1: Tuned to pion scattering data
C
NEUT-MODL 1
C
C
C MODH : Toggle between high energy pion mfp models ( momentum of pi > 500MeV/c )
C                 0: p/n cross sections normalized to pion-deuteron (prior to 2011)
C                 1: Actual p or n cross section used; Intermediate pion charge fixed;
C                    p/n density considered for non-isoscalar nuclei
C
NEUT-MODH 1
C
C KINMODH : Toggle between high energy pion quasielastic scattering models
C           (Only relevant if FEFQEHF > 0)
C                                       ( momentum of pi > 500MeV/c )
C                 0: Isotropic decay of some resonance (Deprecated, do not use)
C                 1: SAID Phase shift analysis + Artificial Fwd. Scatter
C
CNEUT-KINH 1
C
C
C FEFQE : Factor to modify pion quasi-elastic scattering mean free path
C                           ( momentum of pi < 500MeV/c )
NEUT-FEFQE 1.
C
C
C FEFABS : Factor to modify pion absorption mean free path
C          ( Prior to 2011: All MFP scaling = 1.0 )
C          ( Tune to pion scattering data: 1.1 )
NEUT-FEFABS 1.1
C
C
C FEFINEL : Factor to modify pion hadron production mean free path
C                           ( momentum of pi > 500MeV/c )
NEUT-FEFINEL 1.
C
C
C FEFCOH : Factor to modify pion foward scattering mean free path
C                           ( momentum of pi > 500MeV/c )
NEUT-FEFCOH 1.
C
C
C FEFQEH : Factor to modify quasielastic scattering mean free path
C                           ( momentum of pi > 500MeV/c )
C          ( Tune to pion scattering data: 1.8 )
NEUT-FEFQEH 1.8
C
```

```
C
C FEFCX  : Factor to modify charge exchange amplitude
C                           ( momentum of pi < 500MeV/c )
NEUT-FEFCX 1.
C
C
C FEFCXH  : Factor to modify charge exchange mean free path
C                           ( momentum of pi > 500MeV/c )
C          ( Tune to pion scattering data: 1.8 )
NEUT-FEFCXH 1.8
C
C
C FEFQEHF: Portion of QE scattering that has inelastic-like kinematics
C                           ( momentum of pi > 500MeV/c )
C
C NEUT-FEFQEHF 0. ! all forward-like scattering (prior to 2011)
C                ! ( 1 = Tune to pion scattering data, mix of quasielastic
C                         and forward-like scattering)
NEUT-FEFQEHF 1.
C
C
C FEFCXHF: Portion of inel. scattering that includes true CX
C                           ( momentum of pi > 500MeV/c , MODH=1 only)
C
C NEUT-FEFCXHF 0. ! pi+,neutron charge exchange and inelastic
C                  cross sections separated (default)
NEUT-FEFCXHF 0.
C
C
C FEFCOHF: Amount of forward scatter relative to quasi-elastic (p<500)
C
CNEUT-FEFCOHF 0. ! Default, no forward scattering at low momenta
NEUT-FEFCOHF 0.
C
C FEFCOUL: Pion trajectory modified by Coulomb field
C
CNEUT-FEFCOUL 0. ! Default, no Coulomb correction
NEUT-FEFCOUL 0
C
CCCCCCCCCCCCCCCCCCCCCCCCCCCCCCCCCCCCCCCCCCCCCCCCCCCCCCCCCCCCCCCCCCCCCCCCCCCCCCCC
C Nucleon rescattering
C
C NUCRES-RESCAT  1: on (default) 0: off
C
NUCRES-RESCAT 1
C
C NUCRES-XNUCFACT  cross-section factor to study uncertainty default = 1.
C
NUCRES-FACT 1.
C
C
C
C
C MODE : Interaction mode
C                    0 : normal ( default )
C                   -1 : input cross section by CRSNEUT
C                    n : sellect one mode ( n > 0 )   See nemodsel.F
C                          n =  1 : charged current Q.E.
C                          n = 11,12,13
C                                 : charged current Single pi production
C                          n = 16 : coherent Single pi production
C                          n = 21 : charged current Multi pi production
C                          n = 31,32,33,34
C                                 : neutral current Single pi production
```

```
C                          n = 36 : coherent Single pi production
C                          n = 41 : neutral current Multi pi production
C                          n = 51,52 : neutral current elastic
C                          n = 22,42,43 : single eta production
C                          n = 23,44,45 : single  K  production
C
NEUT-MODE   0
C
C  nu                    nub
C  1:     CC Q.E.         CC Q.E.( Free )
C  2-4:   CC 1pi          CC 1pi
C  5:     CC DIS 1320     CC DIS 1.3 < W < 2.0
C  6-9:   NC 1pi          NC 1pi
C  10:    NC DIS 1320     NC DIS 1.3 < W < 2.0
C  11:    NC els          CC Q.E.( Bound )
C  12:    NC els          NC els
C  13:    NC els          NC els
C  14:    coherent        NC els
C  15:    coherent        coherent
C  16:    CC eta          coherent
C  17     NC eta          CC eta
C  18:    NC eta          NC eta
C  19:    CC K            NC eta
C  20     NC K            CC K
C  21:    NC K            NC K
C  22:    N/A             NC K
C  23:    CC DIS          CC DIS (W > 2.0)
C  24:    NC DIS          NC DIS (W > 2.0)
C  25:    CC 1 gamma      CC 1 gamma
C  26,27: NC 1 gamma      NC 1 gamma
C
C
C CRS  :  Multiplied factor to cross section on each mode. ( neu )
C CSRB :  Multiplied factor to cross section on each mode. ( neu-bar )
C
C          1  2  3  4  5  6  7  8  9 10 11 12 13 14 15 16 17 18 19 20 21 22 23 24 25 26 27
NEUT-CRS   1. 0. 0. 0. 0. 0. 0. 0. 0. 0. 0. 0. 0. 0. 0. 0. 0. 0. 0. 0. 0. 0. 0. 0. 0. 0.
NEUT-CRSB  0. 0. 0. 0. 0. 0. 0. 0. 0. 0. 0. 0. 0. 0. 0. 0. 0. 0. 0. 0. 0. 0. 0. 0. 0. 0.
C
C  PDF for DIS is set in this section
C  (GRV94DI -> 7, GRV98_LO -> 12 (default))
CNEUT-PDF    12
C  Which PDF is used ( original=0, modified=1 (default))
CNEUT-BODEK   1
C  Select Coherent pion model (Rein & Sehgal=0(default), Kartavtsev et al.=1
CNEUT-COHEPI  0
C
C  CCQE Axial Mass (For simulation, must be set to: 1.01, 1.11, 1.21{default}. 1.31)
CNEUT-MAQE 1.21
C
C  CC1pi Axial Mass (For simulation, must be set to: 1.21{default}, 1.11)
CNEUT-MASPI 1.21
C
C  CCQE Vector Mass (Default: 0.84)
CNEUT-MVQE 0.84
C
C  CC1pi Vector Mass (Default: 0.84)
CNEUT-MVSPI 0.84
C
C  CCQE Kappa Factor (Default: 1.0)
CNEUT-KAPP 1.0
C
C  Coherent Pion Axial Mass (Default: 1.0)
CNEUT-MACOH 1.0
```

```
C
C  Coherent Pion Nuclear Radios (Default: 1.0 fm)
CNEUT-ROCOH 1.0
C
C MDLQE    : CC Quasi-elastic / NC elastic model
C          : xx1 : Smith-Moniz for CC
C          : xx2 : Smith-Moniz for CC with BBBA05
C          : x0x : Scaling to CCQE     ( same as 5.0.x )
C          : x1x : Scaling to Spectrum func. with Dipole
C          : x2x : Scaling to Spectrum func. with BBBA05
C          : 1xx : Transverse enhancement (0: off, default)
C
NEUT-MDLQE 01
C
C
C RAND : random seed
C      0 : Read RANDOM number from FILE
C      1 : Generating RANDOM SEED from the time
C
NEUT-RAND 1
```

Appendix C

Data tables

C.1 Optimising binning schemes

$\cos\theta$ bin $^{E_\mu}$ bin	1MeV/bin	2MeV/bin	6MeV/bin	10MeV/bin
5e-4/bin	—	—	3.08243 %	—
1e-3/bin	—	—	1.40456 %	—
5e-3/bin	2.08429 %	0.909039 %	0.298813 %	0.218909 %
1e-2/bin	—	—	0.209709 %	—
2e-2/bin	—	—	0.161807 %	—

Table C.1: Percentage of problematic events for the Various binning schemes. The binning scheme (6 MeV/bin, 2e-2/bin) gives the smallest percentage of problematic events while not compromising on the accuracy of the calculation.

z steps	**Type I**	**Type II**	**total**
500	0.0983042 %	0.111405 %	0.209709 %
1000	0.0915039 %	0.120305 %	0.211809 %
5000	0.0858037 %	0.131106 %	0.216909 %
10000	0.0847036 %	0.132606 %	0.217309 %

Table C.2: Percentage of problematic events for the various Z binning schemes. Varying the Z bin size does not affect the percentage of problematic events drastically.

C.2 Values of fractional radiative corrections

$\cos\theta_\mu^{E\mu(GeV)}$	0.1,0.2	0.2,0.3	0.3,0.4	0.4,0.5	0.5,0.6	0.6,0.7	0.7,0.8	0.8,0.9	0.9,1.0	1.0,1.1	1.1,1.2	1.2,1.3	1.3,1.4	1.4,1.5	1.5,1.6	1.6,1.7	1.7,1.8	1.8,1.9	1.9,2.0
+0.9,+1.0	0.14	1.17	1.67	2.11	2.15	1.81	0.76	-0.28	-0.54	-0.43	-0.34	-0.42	-0.29	-0.43	-0.35	-0.54	-0.70	-0.62	-0.84
+0.8,+0.9	0.38	1.30	1.80	2.14	1.99	1.18	-0.46	-2.01	-2.78	-3.40	-4.30	-5.28	-6.45	-8.13	-10.10	-11.78	-14.83	-17.67	-23.79
+0.7,+0.8	0.59	1.34	1.83	2.07	1.65	0.15	-2.42	-4.57	-6.36	-8.64	-12.81	-16.62	-22.87	-31.01	-40.04	-48.37	-57.10	-55.46	-64.22
+0.6,+0.7	0.21	1.38	1.87	1.95	1.11	-1.34	-4.93	-8.47	-12.95	-20.90	-31.79	-42.06	-57.53	-66.85	-70.69	-68.92	-68.28	—	—
+0.5,+0.6	0.36	1.42	1.87	1.74	0.34	-3.54	-8.97	-15.87	-26.17	-46.89	-62.70	-63.76	-70.40	—	—	—	—	—	—
+0.4,+0.5	-0.12	1.44	1.86	1.48	-0.73	-6.52	-15.80	-30.19	-55.34	-65.25	-70.31	-98.55	—	—	—	—	—	—	—
+0.3,+0.4	0.74	1.47	1.82	1.07	-2.26	-11.59	-28.98	-52.76	-75.19	-80.58	—	—	—	—	—	—	—	—	—
+0.2,+0.3	0.60	1.51	1.74	0.56	-4.66	-18.76	-45.91	-68.45	—	—	—	—	—	—	—	—	—	—	—
+0.1,+0.2	0.70	1.53	1.61	-0.05	-8.73	-33.96	-65.18	-83.82	—	—	—	—	—	—	—	—	—	—	—
0.0,+0.1	0.70	1.55	1.43	-1.05	-14.41	-56.20	-75.29	—	—	—	—	—	—	—	—	—	—	—	—
-0.1,0.0	0.77	1.56	1.22	-2.41	-26.95	-64.75	—	—	—	—	—	—	—	—	—	—	—	—	—
-0.2,-0.1	0.82	1.56	0.98	-4.66	-39.97	-77.78	—	—	—	—	—	—	—	—	—	—	—	—	—
-0.3,-0.2	0.83	1.56	0.65	-7.81	-54.93	-88.50	—	—	—	—	—	—	—	—	—	—	—	—	—
-0.4,-0.3	0.86	1.51	0.28	-15.29	-67.54	—	—	—	—	—	—	—	—	—	—	—	—	—	—
-0.5,-0.4	0.80	1.47	-0.20	-21.19	-66.26	—	—	—	—	—	—	—	—	—	—	—	—	—	—
-0.6,-0.5	0.89	1.40	-0.80	-34.34	-79.35	—	—	—	—	—	—	—	—	—	—	—	—	—	—
-0.7,-0.6	0.92	1.34	-1.67	-39.41	—	—	—	—	—	—	—	—	—	—	—	—	—	—	—
-0.8,-0.7	0.99	1.26	-2.81	-51.21	—	—	—	—	—	—	—	—	—	—	—	—	—	—	—
-0.9,-0.8	0.97	1.14	-5.01	-52.89	—	—	—	—	—	—	—	—	—	—	—	—	—	—	—
-1.0,-0.9	0.96	1.02	-8.48	-61.27	—	—	—	—	—	—	—	—	—	—	—	—	—	—	—
Average	0.65	1.40	0.08	-13.92	-22.41	-27.68	-24.72	-29.60	-25.62	-32.30	-30.38	-37.78	-31.51	-30.30	-32.40	-35.23	-24.58	-29.62	

Table C.3: Fractional radiative corrections for ν_μ CCQE interactions. Table shows value of each bin in figure 7.4, expressed as a percentage.

References

[1] Melanie Day and Kevin S. McFarland. Differences in Quasi-Elastic Cross-Sections of Muon and Electron Neutrinos. *Phys.Rev.*, D86:053003, 2012.

[2] Krzysztof M. Graczyk. Relevance of Two Boson Exchange Effect in Quasi-Elastic Charged Current Neutrino-Nucleon Interaction. 2013.

[3] Mark Scott. *Measuring charged current neutrino interactions in the electromagnetic calorimeters of the ND280 detector*. PhD thesis, Imperial College London, 2013.

[4] Kobayashi Takashi and Kee Jung Chang. T2k official website, 2013.

[5] Melody Salzgeber. *Measurement of the Inclusive Neutrino Charged Current Cross Section in the Near Detecor of the T2K Experiment*. PhD thesis, University of Geneva, 2012.

[6] J.E. Kiskis. RADIATIVE CORRECTIONS TO DEEP - INELASTIC NEUTRINO - NUCLEON SCATTERING. *Phys.Rev.*, D8:2129, 1973.

[7] Arie Bodek. Muon internal bremsstrahlung: A Conventional explanation for the excess nu(e) events in MiniBoone. 2007.

[8] Fred L Wilson. Fermi's theory of beta decay. *American Journal of Physics*, 36(12):1150–1160, 1968.

[9] K. Zuber. *Neutrino Physics*. Series in high energy physics, cosmology, and gravitation. Taylor & Francis, 2012.

[10] F.J. Dyson. The Radiation theories of Tomonaga, Schwinger, and Feynman. *Phys.Rev.*, 75:486–502, 1949.

[11] R. P. Feynman and M. Gell-Mann. Theory of the fermi interaction. *Phys. Rev.*, 109:193–198, Jan 1958.

[12] Eo CG Sudarshan and RE Marshak. Chirality invariance and the universal fermi interaction. *Physical Review*, 109(5):1860–1862, 1958.

[13] SS Gershtein and Ia B Zel'dovich. Meson corrections in the theory of beta decay. *Soviet Phys. JETP*, 2, 1956.

[14] Y. K. Lee, L. W. Mo, and C. S. Wu. Experimental test of the conserved vector current theory on the beta spectra of b^{12} and n^{12}. *Phys. Rev. Lett.*, 10:253–258, Mar 1963.

[15] Stephen L. Adler. Tests of the Conserved Vector Current and Partially Conserved Axial-Vector Current Hypotheses in High-Energy Neutrino Reactions. *Phys.Rev.*, 135:B963–B966, 1964.

[16] S.V. Bonetti, E. Fiorini, M. Rollier, et al. Experimental test of the partially conserved axial-vector-current hypothesis. *Lettere al Nuovo Cimento*, 2(18):877–880, 1969.

[17] J Beringer, JF Arguin, RM Barnett, et al. Review of particle physics. *PHYSICAL REVIEW D*, 86(0):1504, 2012.

[18] M. Guidry. *Gauge Field Theories: An Introduction with Applications*. Wiley, 2008.

[19] Julian Schwinger. A theory of the fundamental interactions. *Annals of Physics*, 2(5):407 – 434, 1957.

[20] Roberto Casalbuoni. The standard model of electroweak interactions. Lectures given at the Otranto School, 1997.

[21] ErnestS. Abers and BenjaminW. Lee. Gauge theories. *Physics Reports*, 9(1):1 – 2, 1973.

[22] G. 't Hooft and M. Veltman. Regularization and renormalization of gauge fields. *Nuclear Physics B*, 44(1):189 – 213, 1972.

[23] David J. Gross and R. Jackiw. Effect of anomalies on quasi-renormalizable theories. *Phys. Rev. D*, 6:477–493, Jul 1972.

[24] Adel Bilal. Lectures on anomalies. `arXiv preprint arXiv:0802.0634`, 2008.

[25] Kan Chang Wang. A suggestion on the detection of the neutrino. *Phys. Rev.*, 61:97–97, Jan 1942.

[26] C. L. Cowan, F. Reines, F. B. Harrison, H. W. Kruse, and A. D. McGuire. Detection of the free neutrino: a confirmation. *Science*, 124(3212):103–104, 1956.

[27] Y. Fukuda, T. Hayakawa, E. Ichihara, et al. Evidence for oscillation of atmospheric neutrinos. *Phys. Rev. Lett.*, 81:1562–1567, Aug 1998.

[28] P.A.R. Ade et al. Planck 2013 results. I. Overview of products and scientific results.

Astronomy and Astrophysics, 2013.

[29] Ariel Goobar, Steen Hannestad, Edvard Mortsell, and Huitzu Tu. A new bound on the neutrino mass from the sdss baryon acoustic peak. *JCAP*, 0606:019, 2006.

[30] Ilia Gogoladze, Nobuchika Okada, and Qaisar Shafi. NMSSM and seesaw physics at LHC. *Physics Letters B*, 672(3):235 – 239, 2009.

[31] Roberto Franceschini, Thomas Hambye, and Alessandro Strumia. Type-III seesaw mechanism at CERN LHC. *Phys. Rev. D*, 78:033002, Aug 2008.

[32] B. Pontecorvo. Mesonium and anti-mesonium. *Sov.Phys.JETP*, 6:429, 1957.

[33] Carlo Giunti. *Fundamentals of neutrino physics and astrophysics.* Number 34A5427. Oxford University Press, 2007.

[34] G. Zacek, F. v. Feilitzsch, R. L. Mössbauer, et al. Neutrino-oscillation experiments at the gösgen nuclear power reactor. *Phys. Rev. D*, 34:2621–2636, Nov 1986.

[35] A.I. Afonin, S.A. Bogatov, A.G. Vershinsky, et al. ANTI-ELECTRON-NEUTRINO SPECTRA AT TWO DISTANCES FROM THE REACTOR OF THE ROVNO NUCLEAR POWER PLANT: SEARCH FOR OSCILLATIONS. *JETP Lett.*, 45:247–251, 1987.

[36] P. Astier et al. Search for nu(mu) - nu(e) oscillations in the NOMAD experiment. *Phys.Lett.*, B570:19–31, 2003.

[37] E. Eskut, A. Kayis-Topaksu, G. Onengüt, et al. New results from a search for nu(mu)-nu(tau) and nu(e)-nu(tau) oscillation. *Physics Letters B*, 497(1–2):8 – 22, 2001.

[38] B. Armbruster et al. Upper limits for neutrino oscillations muon-anti-neutrino to electron-antineutrino from muon decay at rest. *Phys.Rev.*, D65:112001, 2002.

[39] A. Aguilar-Arevalo et al. Evidence for neutrino oscillations from the observation of anti-neutrino(electron) appearance in a anti-neutrino(muon) beam. *Phys.Rev.*, D64:112007, 2001.

[40] J. Dorenbosch et al. EXPERIMENTAL RESULTS ON NEUTRINO - ELECTRON SCATTERING. *Z.Phys.*, C41:567, 1989.

[41] M. Apollonio et al. Search for neutrino oscillations on a long baseline at the CHOOZ nuclear power station. *Eur.Phys.J.*, C27:331–374, 2003.

[42] F. Boehm, J. Busenitz, B. Cook, et al. Final results from the Palo Verde neutrino oscillation experiment. *Phys.Rev.*, D64:112001, 2001.

[43] Y. Itow et al. The JHF-Kamioka neutrino project. pages 239–248, 2001.

[44] P. Adamson et al. First direct observation of muon antineutrino disappearance. *Phys.Rev.Lett.*, 107:021801, 2011.

[45] Y. Ashie et al. Evidence for an oscillatory signature in atmospheric neutrino oscillation. *Phys.Rev.Lett.*, 93:101801, 2004.

[46] Mayly C. Sanchez et al. Measurement of the L/E distributions of atmospheric neutrinos in Soudan 2 and their interpretation as neutrino oscillations. *Phys.Rev.*, D68:113004, 2003.

[47] B.T. Cleveland, Timothy Daily, Jr. Davis, Raymond, et al. Measurement of the solar electron neutrino flux with the Homestake chlorine detector. *Astrophys.J.*, 496:505–526, 1998.

[48] S.N. Ahmed et al. Measurement of the total active B-8 solar neutrino flux at the Sudbury Neutrino Observatory with enhanced neutral current sensitivity. *Phys.Rev.Lett.*, 92:181301, 2004.

[49] J. Beringer et al. Review of Particle Physics (RPP). *Phys.Rev.*, D86:010001, 2012.

[50] U. SARKAR and H. V. KLAPDOR-KLEINGROTHAUS. Implications of observed neutrinoless double beta decay. *Modern Physics Letters A*, 16(38):2469–2482, 2001.

[51] L. Bornschein. The {KATRIN} experiment - a direct measurement of the electron antineutrino mass in the sub-ev region. *Nuclear Physics A*, 752(0):14 – 23, 2005. Proceedings of the 22nd International Nuclear Physics Conference (Part 2).

[52] DE Groom, Particle Data Group, et al. Eur. *Phys. Jour C*, 15:1, 2000.

[53] David O. Caldwell. LSND results and their consequences. 1995.

[54] X. Qian, C. Zhang, M. Diwan, and P. Vogel. Unitarity Tests of the Neutrino Mixing Matrix. 2013.

[55] Samantha Short. *Study of Neutrino-Induced Neutral Current Neutral Pion Production in the T2K Near Detector.* PhD thesis, Imperial College London, 2013.

[56] T2K Collaboration, K. Abe, N. Abgrall, et al. The T2K experiment. *Nuclear Instruments and Methods in Physics Research A*, 659:106–135, December 2011.

[57] Teppei Katori. *A Measurement of the muon neutrino charged current quasielastic interaction and a test of Lorentz violation with the MiniBooNE experiment.* PhD thesis, Indiana University, 2008.

[58] C.H. Llewellyn Smith. Neutrino reactions at accelerator energies. *Physics Reports*,

3(5):261 – 379, 1972.

[59] J. Arrington. How well do we know the electromagnetic form factors of the proton? *Phys. Rev. C*, 68:034325, Sep 2003.

[60] A Pais. Weak interactions at high energies. *Annals of Physics*, 63(2):361 – 392, 1971.

[61] E.D. Commins and P.H. Bucksbaum. *Weak Interactions of Leptons and Quarks*. 1983.

[62] Neutrino reactions on nuclear targets: R.a. smith and e.j. moniz, nucl. phys. {B43} (1972) 605. *Nuclear Physics B*, 101(2):547 –, 1975.

[63] Omar Benhar, Donal day, and Ingo Sick. Inclusive quasi-elastic electron-nucleus scattering. *Rev.Mod.Phys.*, 80:189–224, 2008.

[64] O. Benhar, N. Farina, H. Nakamura, M. Sakuda, and R. Seki. Lepton-nucleus scattering in the impulse approximation regime. *Nucl.Phys.Proc.Suppl.*, 155:254–256, 2006.

[65] M.E. Peskin and D.V. Schroeder. *Introduction to Quantum Field Theory*. Levant Books, 2005.

[66] D. Hanneke, S. Fogwell Hoogerheide, and G. Gabrielse. Cavity control of a single-electron quantum cyclotron: Measuring the electron magnetic moment. 83(5):052122, May 2011.

[67] F. Bloch and A. Nordsieck. Note on the radiation field of the electron. *Phys. Rev.*, 52:54–59, Jul 1937.

[68] M. Kaku. *Quantum Field Theory: A Modern Introduction*. Oxford University Press, 1993.

[69] A. De Rújula, R. Petronzio, and A. Savoy-Navarro. Radiative corrections to high-energy neutrino scattering. *Nuclear Physics B*, 154(3):394 – 426, 1979.

[70] Y. Hayato. Neut. *Nuclear Physics B - Proceedings Supplements*, 112(1–3):171 – 176, 2002.

[71] K. Abe et al. Measurement of the Inclusive muon neutrino Charged Current Cross Section on Carbon in the Near Detector of the T2K Experiment. *Phys.Rev.*, D87:092003, 2013.